Advancing Discrimination Performance by integrating an Inertial Measurement Unit with a handheld EMI Sensor

ESTCP MM-0810
Interim Technical Report
APG Standardized UXO Test Site

July 2012

Report Documentation Page

Form Approved
OMB No. 0704-0188

1. REPORT DATE	2. REPORT TYPE	3. DATES COVERED
JUL 2012	**N/A**	**-**

4. TITLE AND SUBTITLE	5a. CONTRACT NUMBER
Advancing Discrimination Performance by integrating an Inertial Measurement Unit with a handheld EMI Sensor	5b. GRANT NUMBER
	5c. PROGRAM ELEMENT NUMBER
6. AUTHOR(S)	5d. PROJECT NUMBER
	5e. TASK NUMBER
	5f. WORK UNIT NUMBER
7. PERFORMING ORGANIZATION NAME(S) AND ADDRESS(ES) **ESTCP Office 4800 Mark Center Drive Suite 17D08 Alexandria, VA 22350-3605**	8. PERFORMING ORGANIZATION REPORT NUMBER
9. SPONSORING/MONITORING AGENCY NAME(S) AND ADDRESS(ES)	10. SPONSOR/MONITOR'S ACRONYM(S)
	11. SPONSOR/MONITOR'S REPORT NUMBER(S)

12. DISTRIBUTION/AVAILABILITY STATEMENT
Approved for public release, distribution unlimited

13. SUPPLEMENTARY NOTES
The original document contains color images.

14. ABSTRACT

15. SUBJECT TERMS

16. SECURITY CLASSIFICATION OF:			17. LIMITATION OF ABSTRACT	18. NUMBER OF PAGES	19a. NAME OF RESPONSIBLE PERSON
a. REPORT	b. ABSTRACT	c. THIS PAGE			
unclassified	**unclassified**	**unclassified**	**SAR**	**84**	

Contents

Figures

Tables

Acronyms

APG	Aberdeen Proving Ground
ATC	Aberdeen Test Center
DMC	Digital Magnetic Compass
EMI	Electromagnetic Induction
ESTCP	Environmental Security Technology Certification Program
GPS	Global Positioning System
IMU	Inertial Measurement Unit
MEMS	Micro Electro-Mechanical Systems
MTADS	Multi-sensor Towed Array Detection System
NRL	Naval Research Laboratory
PC	Personal Computer
POC	Point of Contact
QC	Quality Control
R-T-S	Rauch-Tung-Streibe
SAINT	Small Area Inertial Navigation Tracking
SBC	Single Board Computer
SERDP	Strategic Environmental Research and Development Program
SNR	Signal-to-Noise Ratio
USAEC	U.S. Army Environmental Command
UXO	Unexploded Ordnance
ZUPT	Zero velocity Update

1.0 EXECUTIVE SUMMARY

We compared classification capabilities for handheld electromagnetic sensors that were deployed using either a grid-based template for spatial registration or an IMU-based positioning system. Demonstration data were collected at the Aberdeen Proving Ground using both systems. The two data sets were analyzed separately and submitted to the Institute for Defense Analyses for grading.

The IMU-based positioning system involved in this demonstration is known as the Small Area Inertial Navigation and Tracking (SAINT) system. It was developed by ENSCO as part of an earlier ESTCP project and enhanced and integrated with the EM61HH sensor in support of this effort. The SAINT system consists of a Honeywell HG1900 IMU and a LEICA DMC. The Honeywell HG1900 IMU consists of orthogonally aligned MEMS accelerometers and gyroscopes that record 3-axis acceleration and rotation rates, respectively enclosed in an 8-cubic inch container. The LEICA DMC is employed to aid the IMU and constrain heading drift. The digital magnetic compass measures the strength and direction of a magnetic field and can be used to determine magnetic north in an environment free of additional magnetic fields. SAINT records all IMU and digital magnetic compass data onto an internal compact flash card.

The concept of operations for the SAINT+EMI sensing system consists of the following steps; initial zero velocity update (ZUPT), acquire data, final ZUPT. During the initial ZUPT, the SAINT unit is set down on the tripod mount and remains stationary for 15 seconds. During data collection, the operator picks up the unit and acquires geophysical data for 30 seconds or less of free navigation over the area of interest. The data collection event ends when the SAINT unit is returned to its original location on the tripod mount for about 15-seconds final ZUPT.

The template consisted of a 6 by 6 square grid of points with a spacing of 0.15 m. Each grid had 38 measurements with the first and last being in the air to zero the sensor. Template measurements took roughly 3-4 minutes a cell with a comparable average daily rate to the SAINT. Logistically, the wooden template had to be moved cell to cell which was comparable to moving the SAINT tripod cell to cell. Both the SAINT and template data were fit with the same EMI model. Discrimination decisions were based on the same library fit and ratio test.

Overall, excellent response stage and discrimination stages results were obtained for both positioning systems. For the response stage, the EM61-HH was manually swept over the center of each cell. If there was no measurable signal (~ 10 mV) within roughly 0.25 m of the cell center, the cell was determined to be empty for both data sets and no further measurements were taken. The EM61-HH missed only 105mm's (projectile and HEAT) and only at their deepest depth range (8-12 times their diameter) with a P_d of 0.67 in this range. All other P_d's were 1.0 with an overall P_d of 0.99.

The template data and SAINT data were processed with the same discrimination algorithm with the same threshold settings. The template data achieved an overall discrimination stage P_d of 0.93 compared to 0.99 for the SAINT. With regard to efficiency, which is a measure of how much of the ordnance detected was identified as ordnance in the discrimination stage, the SAINT system identified all detected ordnance as being ordnance and had a score of 1.0 while the template's score was 0.93.

2.0 INTRODUCTION

2.1 BACKGROUND

The billion-plus estimated cost of cleaning up land contaminated with unexploded ordnance (UXO) and related materials is significantly affected by the costs associated with excavating objects that pose no harm. The Defense Science Board has calculated that if the false alarm rate can be reduced from 100:1 to 10:1, the economics of UXO remediation can be inverted from 75% of the cost devoted to digging false alarms to 75% devoted to digging UXO [1].

Differentiating between UXO and clutter using shape information derived from electromagnetic induction (EMI) data has proven difficult during the past decade. Although notable success has been realized by the research community using data acquired in very controlled settings, errors inherent with spatially registering field data have significantly limited discrimination performances. It turns out that position estimates possessing sub-centimeter precision are required. When combined with data density challenges, signal-to-noise issues, and non-unique solutions, these issues have dramatically tempered discrimination performances. The impact on the Department of Defense is clear - and expensive. The widespread view that discrimination is not possible drives the requirement that all detected objects must be removed. This in turn, drives the total cleanup cost, which is estimated in the billions of dollars. This project was directed towards demonstrating improved discrimination performances in field settings by precisely spatially registering handheld EMI sensor measurements using a tactical grade inertial navigation tracking system.

The current approach to mitigating sensor positioning problems associated with dynamic surveys involves collecting data on a fixed grid over the target using a template laid on the ground. Although inexpensive, this approach leaves much to be desired. A more desirable positioning solution is one that is integral to the sensor, allows the operator to sweep the sensor back and forth with ease, and permits the data density to be dynamically adjusted. This would permit use in rougher terrain and confined locations. This project integrates a tactical grade inertial navigation and tracking system with a commercial EM61HH-MK2 sensor. The inertial navigation tracking system developed by ENSCO consists of a Honeywell HG1900 inertial measurement unit (IMU) and a LEICA digital magnetic compass and has demonstrated sub centimeter precision. The EM61HH-MK2 is a hand-held complement to the EM61-MK2, providing greater sensitivity to smaller targets at shallow depths.

2.2 OBJECTIVE OF THE DEMONSTRATION

Our objective is to establish classification performance for a handheld data collection system that combines an EMI sensor and an IMU.

2.3 REGULATORY DRIVERS

Stakeholder acceptance of the use of discrimination techniques on real sites will require demonstration that these techniques can be deployed efficiently and with high probability of discrimination. The first step in this is to demonstrate acceptable performance on a test site such as that at Aberdeen. After that hurdle has been passed, successful demonstration at a live site will facilitate regulatory acceptance of the methods.

3.0 TECHNOLOGY

3.1 TECHNOLOGY DESCRIPTION

The principal objective of this demonstration is to successfully classify obscured UXO targets by inverting geophysical data that are spatially positioned using an IMU, which precisely positions geophysical measurements, relative to each other, as they acquired as a function of time. To accomplish this objective, we leveraged ENSCO's Small Area Inertial Navigation and Tracking (SAINT; Figure 3-1). The photos (from left to right) show a SAINT-aided EM61HH being used on a wooden platform designed for routine testing. The concept of operation (CONOPS) includes setting the sensing system (EM61/SAINT plus tripod) within a meter or two of an anomaly location. The SAINT is rigidly attached to the EM61 handle. The combined system is placed on a tripod and powered up. After sitting idle for 15 seconds of background data, the SAINT beeps once and flashes the blue LED. The user lifts the system and proceeds to sweep the sensor back and forth over the object location. The SAINT beeps and flashes at several intervals during data collection. After 30 seconds of collection it beeps and lights up continuously until replaced on the tripod. After another 15 seconds of being idle, it beeps/flashes once to indicate that it is ready to move again. Examples of actual sweep data are shown below the photos below. After the idle period, more data can be collected over the same object or from nearby objects without moving the tripod if desired.

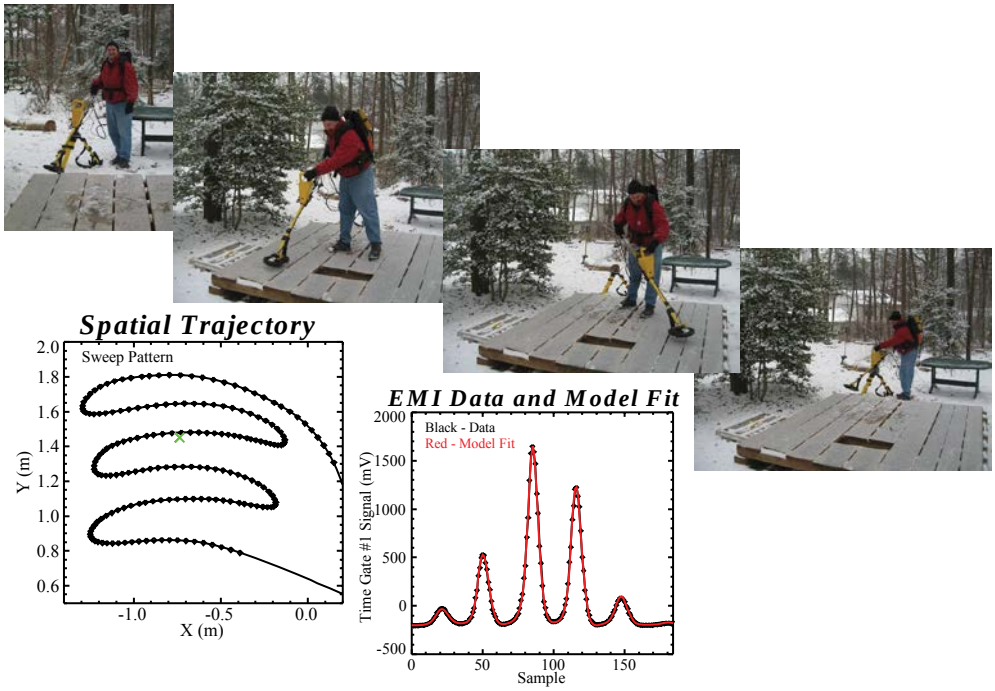

Figure 3-1 Standard survey procedures include taking the sensor off of the tripod, waving it above the targets' location, and returning the sensor to the tripod for a zero velocity update (top photographs). The two scatter plots on the bottom show the spatial trajectory of the sensor head (bottom left) and the measured EMI data (bottom right).

3.1.1 EMI Sensor – EM61HH

We utilized an EM61HH sensor manufactured by Geonics. The EM61HH is a hand-held complement to the EM61, providing greater sensitivity to smaller targets at shallow depths. Data is collected from an air-core, 17cm diameter, single receive coil at four time gates, geometrically spaced in time from 147 μs to 613 μs, after transmitter turn-off. With a smaller spatial footprint than the standard EM61, the EM61HH is relatively less sensitive to sources of potential interference. The small footprint also provides enhanced target resolution and, consequently, improves discrimination of multiple targets.

Effective cued identification using the EM61HH has been demonstrated by AETC in ESTCP project 200108 (Handheld Sensor for Unexploded Ordnance Discrimination). As reported at the 2002 SERDP/ESTCP Partners in Environmental Technology Symposium, the sensor technology was demonstrated at a Brownfield Redevelopment site and achieved excellent results in discriminating between UXO items (37mm, 47mm and 75mm projectiles) and various industrial and cultural clutter items [2]. For that demonstration, the sensor positioning problem was solved by collecting data on a fixed grid over the target using a template laid on the ground (Figure 3-2).

Figure 3-2 A standard approach to mitigating sensor positioning problem involves collecting data on a fixed grid over the target using a template laid on the ground. The sensor in the photograph is an EM61HH-MK2.

3.1.2 Data Analysis

The basic electromagnetic induction response model involves a simple dipole response [3]. Inversion of this model solves for the object's location, object orientation, and the magnetic polarization response terms. The polarization terms, referred to here as β's, determine the strength of the object's induced response along the object's physical axes. It is these terms that allow for discrimination between buried ordnance and other metallic clutter. For elongated ferrous ordnance items such as a projectile or mortar, there is one large, primary β response along the item's long axis and two smaller, secondary responses transverse to this $\beta_x > \beta_y = \beta_z$. Accurately determining these parameters from model-based inversion is limited by the signal-to-noise ratio of the sensor data and by the positioning accuracy of the sensor trajectory. In fact, simulations suggest that positioning accuracies of better than one centimeter are required to invert β's with less than 20% error.

When sweeping the EM61HH back and forth over a target, it has been previously noted [5] that the peak EM61HH response was both delayed and distorted relative to the actual target location. The receiver output of this sensor is analog integrated with a filter that both shifts and distorts the sensor's response. This filter can sufficiently distort signal shape to limit the inversion process. This impacts the accuracy of target parameter estimates from dipole inversion at sweeping speeds of more than a few cm/sec. At such speeds, it is necessary to account for the sensor's temporal response. Figure 3-3 compares inversion results with the static (upper plot) and dynamic (lower plot) response models. In these figures, the primary (largest) β is plotted along the horizontal axis, and the secondary βs are plotted along the vertical axis, with a symbol at the mean value and a line running between the two. For the test objects (two spheres and two projectiles), the two transverse beta values are expected to be equal. Furthermore, for the two spheres considered, all three betas (i.e. longitudinal and transverse) are expected to be equal. The dotted line represents the line where longitudinal and transverse values are equal. The dynamic model generally produces tighter eigenvalue clusters and better shape characterization (secondary βs more nearly equal) than does the static model.

Using empirical tests, the sensors' temporal response was determined and incorporated into the dipole inversion models used for this demonstration.

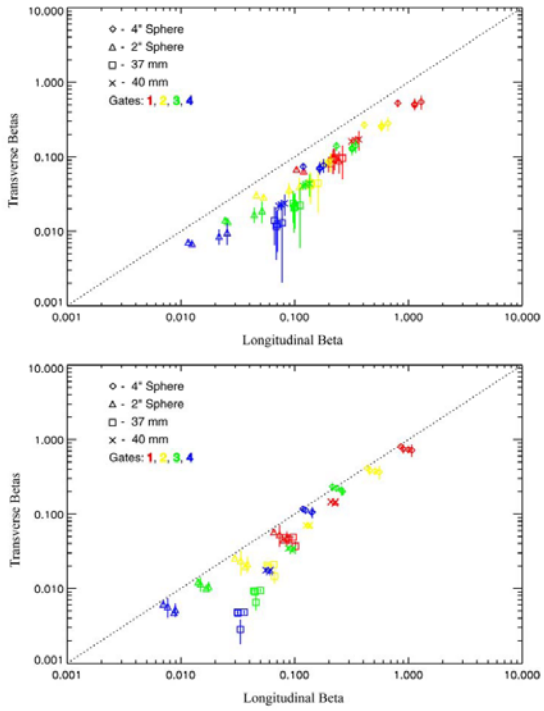

Figure 3-3 Inversion results showing polarizations (β's) when the dynamic response is not taken into account (top) versus when it is taken into account (bottom).

3.1.3 Spatial Registration System

For recording the sensors 3-D position, we used ENSCO's SAINT system, which was originally developed in 2007 [4] and enhanced during this program. It is a stand-alone

unit (Figure 3-4). The inertial navigation tracking system consists of a Honeywell HG1900 inertial measurement unit (IMU) and a LEICA digital magnetic compass (DMC). The Honeywell HG1900 IMU consists of orthogonally aligned micro electro-mechanical systems (MEMS) accelerometers and gyroscopes that record 3-axis acceleration and rotation rates, respectively enclosed in an 8-cubic inch container. The LEICA DMC is employed to aid the IMU and constrain heading drift. The digital magnetic compass measures the strength and direction of a magnetic field and can be used to determine magnetic north in an environment free of additional magnetic fields. With the exception of batteries, a tripod stand, and the post-processing personal computer (PC), all components of SAINT are packaged into a single enclosure. The prototype SAINT system [4, 5] achieved spatial registration accuracies of <1cm.

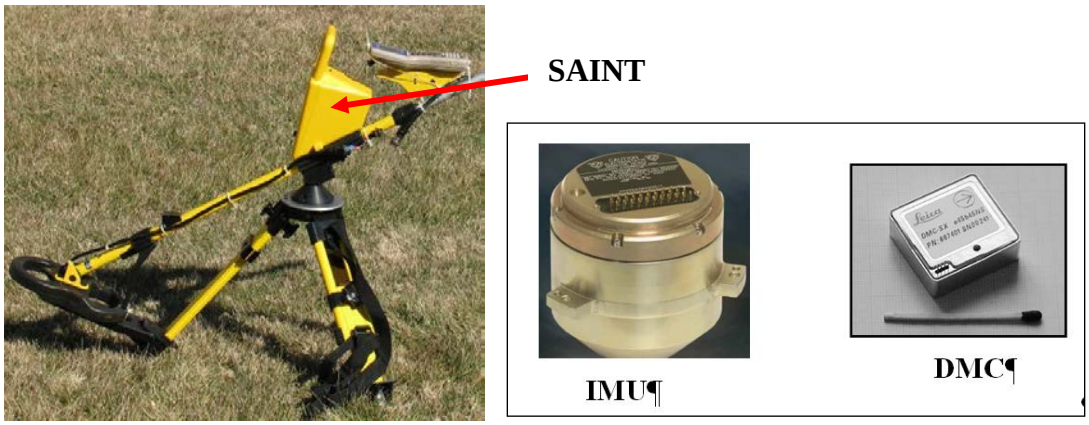

Figure 3-4 Left: SAINT attached to the handle of an EM61HH-MK2. Right: Honeywell HG1900 IMU and LEICA DMC, which are housed within the yellow enclosure.

As part of this project, we built an improved SAINT sensor and integrated it fully with the EM61HH sensor. The changes made significant structural changes to SAINT in order to make the system more efficient and fieldable while still maintaining the original systems accuracy and ease of use (Figure 3-5 and Figure 3-6). The improvements included (i) mitigating synchronization timing issues between the SAINT and EM61HH; (ii) migrating the data acquisition software from an embedded processor to a single board computer (SBC); (iii) redesigning the hardware for easier access; (iv) fabricating a non-metallic docking station; and (v) improving the calibration procedures. See Appendix A for details regarding the system improvements and validation tests.

	Prototype	Test Run #1	Test Run #2
X	0.009	0.004	0.004
Y	0.006	0.008	0.005
Z	0.002	0.003	0.003

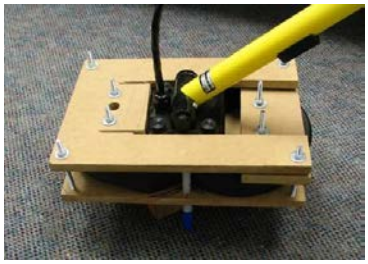

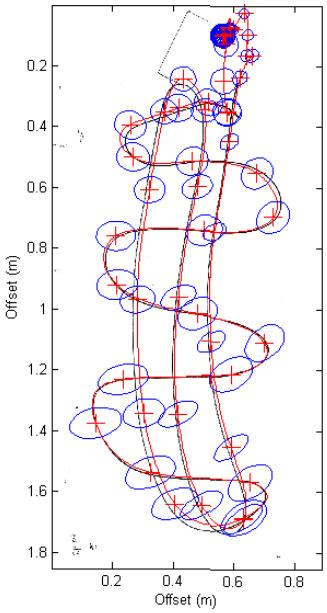

Figure 3-5 A comparison of the actual (2-D motion, pen trace on paper) versus the computed position from the SAINT system. Top right: The black line represents the actual path, and the red line represents the path estimated using the R-T-S Smoother. The blue ellipses correlate to the 95% confidence errors estimated by post-processing software.

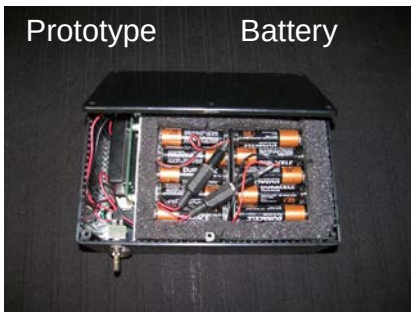

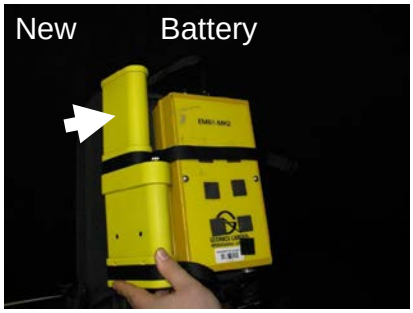

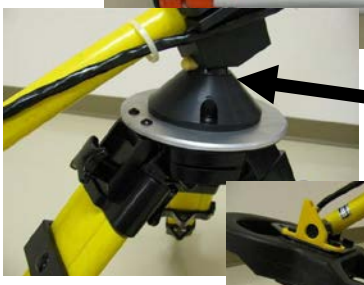

redesigned

ZUPT mount

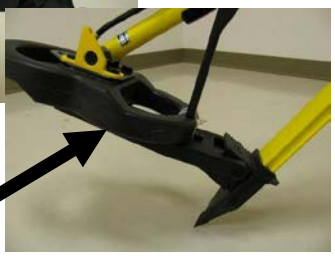

sensor head rest

during ZUPT

Figure 3-6 The battery (left) and tripod (right) were redesigned during this project.

3.2 ADVANTAGES AND LIMITATIONS OF THE TECHNOLOGY

The SAINT positioning system was integrated with the EM61HH sensor and records position data with the sensor data. The advantage of the SAINT compared to the traditional grid template method is the ability to sweep the sensor back and forth with ease and dense and varied data collections and sweep patterns. This is especially valuable for large footprint anomalies because a larger spatial grid (out to the background) can be collected whereas this is not feasible or efficient using a fixed template. Similarly, for smaller targets the sensor can be moved slower over a smaller area to increase the data density over the target.

The SAINT would permit use in rougher terrain and confined locations that may not be conducive to placing a rigid template on the ground. Many times vegetation or other natural obstructions, such as rocks and stumps, do not allow a grid template to be placed securely on the ground. The ability of the SAINT system to sweep around these obstructions is significant advantage when surveying in a treed environment.

Another advantage of the SAINT system is data production rate. It is anticipated that an operator can interrogate twice as many targets compared to the grid template method during a fixed period of time. The position data will also be more reliable as operator fatigue and error are more pronounced using the grid template. Over the course of the day and project, sensor operators tend to be less careful when placing the sensor on the grid template. Also, the operator may accidentally skip or add grid nodes when using the grid template. Most of the time it is impossible to tell with certainty which grid nodes were skipped during collection so the data is discarded and the target is resurveyed. Using the SAINT system should alleviate these problems.

The main limitation of the SAINT system is the duration of free navigation time before the system must be set down and a zero velocity update (ZUPT) performed. Longer data collection times would facilitate use and decrease total operation time. IMU position errors grow quadratically with the duration of free navigation between ZUPTs. For a given IMU, shorter free navigation leads to smaller maximum errors, longer free navigation leads to larger free navigation errors. A better quality IMU would extend the useable free navigation time and/or reduce the maximum error. We selected the HG1900 as a tradeoff between price, size/weight, and performance of available IMUs.

This demonstration used an EM61HH sensor with the hand-held coils which is a standard commercial UXO sensor. The size of coils makes it easy to move the sensor and collect cued data. Unfortunately, the transmit power and smaller coil size also limit the sensors ability to detect most ordnance at their maximum burial depth.

A known limitation to the data analysis results from non-unique inversion results. Using EMI data, an estimate of the objects' shape can be made. Specifically, the eigenvalues of the magnetic polarizability tensor provide the shape information. There are three eigenvalues – each corresponds to a principal axis of object. Discrimination is possible only to the degree that the eigenvalues are different. In other words, even with ideal data, the estimated burial depth, apparent size, and shape features may not separate UXO and

clutter signatures into distinct, non-overlapping classes. This is because the anomaly features derived from EMI and magnetic data are not necessarily unique to UXO. Clutter items that have similar shapes and burial attributes to ordnance can have geophysical signatures that are indistinguishable from UXO signatures and, as such, will have similar eigenvalues and therefore likely be classified as ordnance. Examples include items such as pipes, post sections and axial symmetrical fragments.

4.0 PERFORMANCE OBJECTIVES

The performance objectives for this demonstration are summarized in Table 4-1.

Table 4-1. Performance Objectives for This Demonstration

Performance Objective	Metric	Data Required	Success Criteria	Performance
Quantitative Performance Objectives				
Maximize correct classification of UXO	Number of UXO retained	• Ranked Anomaly list • Scoring report	Approach correctly classifies >95% of UXO	Yes
Maximize correct classification of clutter	Number of false alarms eliminated at demonstrator operating point.	• Ranked anomaly lists • Scoring report	Reduction of false alarms by > 40% while retaining >95% of detected munitions	Yes
Production Rate	Number of targets interrogated each day	• Log of field work	2x the number of targets using grid template	No
Qualitative Performance Objective				
Ease of Use		• Feedback from operator on ease of use		Yes

4.1 OBJECTIVE: MAXIMIZE CORRECT CLASSIFICATION OF UXO

This is one of the two primary measures of the effectiveness of the classification approach. By collecting high-quality data and analyzing those data with advanced parameter estimation and classification algorithms we expect to be able to classify the targets with high efficiency.

4.1.1 Metric

The metric is the number of UXO items that were correctly classified as UXO

4.1.2 Data Requirements

Data requirements include ground truth information and inverted features.

4.1.3 Success Criteria

The objective was considered met if <95% of the UXO are correctly labeled as UXO.

4.2 OBJECTIVE: MAXIMIZE CORRECT CLASSIFICATION OF CLUTTER

This is a primary measure of the effectiveness. By collecting high-quality, precisely-located data, we were able to discriminate detectable munitions from scrap and frag with high efficiency.

4.2.1 Metric

We compared the number of false targets that can be eliminated using the demonstrated discrimination procedures for both the SAINT and grid template positioned data to the total number of false targets. We prepared a ranked dig list for the targets we interrogate with a dig/no-dig threshold indicated and ATC personnel used their automated scoring algorithms to assess our results.

4.2.2 Data Requirements

The identification of the items in the test field is known to the test site operators. Our ranked dig list is the input for this standard and ATC's standard scoring is the output.

4.2.3 Success Criteria

The objective was considered met if the SAINT positioned data performed equal to or better than the grid template data. Additionally, for the anomalies that have a SNR sufficient for analysis, eliminating more than 40% of the non-munitions items while retaining 95% of the munitions items on the dig list was deemed a success.

4.3 OBJECTIVE: PRODUCTION RATE

One of the objectives of using the SAINT to position the sensor is to increase the number of targets that are investigated each day. The increase in production should outweigh the increased cost of the equipment.

4.3.1 Metric

The number of targets interrogated per day is the metric for this objective. We compared the number using the SAINT positioned system to the traditional grid template.

4.3.2 Data Requirements

Survey productivity will be determined from a review of the demonstration field logs.

4.3.3 Success Criteria

The objective was considered met if at least twice as many targets are interrogated each survey day using the SAINT positioned system.

4.4 OBJECTIVE: EASE OF USE

This qualitative objective was intended as a measure of the long-term usability of the technology.

4.4.1 Data Requirements

This objective was evaluated based on operator feedback

5.0 SITE DESCRIPTION

5.1 SITE SELECTION

This demonstration was conducted at the APG Standardized UXO Technology Demonstration Site located at the Aberdeen Proving Ground, MD. Use of this site allowed us to receive validation results from near-real-world conditions without incurring the logistics and intrusive investigation expenses that is required for a demonstration at a live site.

5.2 SITE HISTORY

The APG Standardized Test Site is located within a secured range area of the Aberdeen Proving Grounds. The Aberdeen Area of APG is located approximately 30 miles northeast of Baltimore at the northern end of the Chesapeake Bay. The Standardized UXO Technology Demonstration Site is adjacent to the Trench Warfare facility at the Aberdeen Proving Ground. The specific area was used for a variety of ordnance tests over the years. Initial magnetometer and EMI surveys conducted by the MTADS team performed after a "mag and flag" survey of the same area identified over a thousand remaining anomalies. These data were used for a final clean up of the site prior to the emplacement of the original test items. Prior to the two subsequent reconfiguration events, unexplained anomalies identified by demonstrators using the site were also investigated and removed.

5.3 SITE TOPOGRAPHY AND GEOLOGY

The demonstration site is relatively flat and conducive to acquiring high quality geophysical data. The local near surface materials consist of very deep, slowly permeable, poorly drained soils [6]. Slopes range from 0 to 2 percent.

5.4 MUNITIONS CONTAMINATION

The area currently occupied by the Standardized site has seen an extensive history of munitions use. Historical records provided by ATC and previous remediation results indicated that the likely munitions of interest for this site are:

- Grenades, MkI, MkII, and French VB Rifle without chute
- Grenades, French VB Rifle w/ chute
- 60mm mortars (including 2" Smoke)
- 3" Stokes (Smoke and HE)
- 105 mm projectiles
- 155 mm projectiles

5.5 SITE GEODETIC CONTROL INFORMATION

There are two first-order survey points on the site for use as GPS base station points (see Table 5-1 for details). The horizontal datum for all values is NAD83. The vertical control is referenced to the NAVD88 datum and the Geoid03 geoid.

Table 5-1: Geodetic control at the APG Demonstration Site

ID	Latitude	Longitude	Elevation	Northing	Easting	HAE
477	39º 28' 18.63880" N	76º 07' 47.71815"W	10.669 m	4,369,749.013	402,810.038	-22.545
478	39º 28' 04.24219" N	76º 07' 48.50439"W	11.747 m	4,369,305.416	402,785.686	-21.473

5.6 SITE CONFIGURATION

Figure 5-1 is a map of the Standardized UXO Technology Demonstration Site at APG. The Calibration and Blind Grids are shown along with the various Open Field Areas.

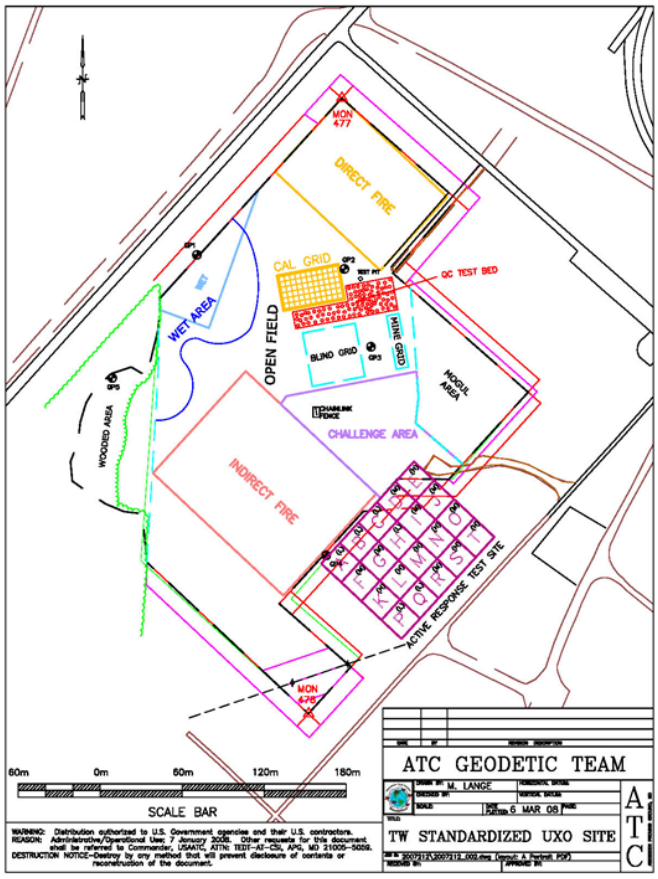

Figure 5-1 Map of the APG Standardized UXO Test Site.

6.0 TEST DESIGN

6.1 CONCEPTUAL EXPERIMENTAL DESIGN

The demonstration was executed in two stages. The first stage included collecting cued EM61HH data using a grid template while the second stage used the SAINT to position the sensor head.

The data from both the template positioned and SAINT positioned surveys were inverted using the data analysis methodology discussed in Section 7. Estimated target parameters as well as the classification decisions were submitted to AEC for scoring.

6.2 SITE PREPARATION

The Standardized UXO Test Sites are configured with clearly-marked calibration, blind validation, and open field scenarios. Two GPS control points are also provided. Basic facilities such as portable toilets and field buildings are also provided. No additional or special site preparation was required for this demonstration.

6.3 SYSTEMS SPECIFICATION

6.3.1 Time-domain EMI Sensor

The EM61HH was used for this demonstration. We configured the sensor to record the four standard factory-programmed time gates (0.147ms, 0.263ms, 0.414ms and 0.613ms).

6.3.2 Grid Template

The EMI data were collected on a 6x6 point square grid (nodes separated by 15cm resulting in a 75x75cm area). The grid template was placed directly on the ground, with the EM61HH positioned directly on the grid (Figure 6-1). Sensor location on the grid was controlled by attaching a plexiglass guide with crosshairs to the bottom of the sensor coils and lining up the cross hairs with grid line intersections. EM61HH data were recorded using the handheld field computer and software that is part of the standard equipment package. The software was set to record all data for each target in one survey line with the data file consisting of multiple survey lines. The data were recorded continuously for each target at 10 readings/second and the fiducial marker used to flag the times when the sensor is at rest over each grid node.

Figure 6-1: Template used to collect EM61HH array data during reacquisition.

6.3.3 SAINT

The SAINT system consists of a Honeywell HG1900 IMU and a LEICA DMC. The Honeywell HG1900 IMU consists of orthogonally aligned MEMS accelerometers and gyroscopes that record 3-axis acceleration and rotation rates, respectively enclosed in an 8-cubic inch container. The LEICA DMC is employed to aid the IMU and constrain heading drift. The digital magnetic compass measures the strength and direction of a magnetic field and can be used to determine magnetic north in an environment free of additional magnetic fields. SAINT records all IMU and digital magnetic compass data onto an internal compact flash card (CF).

Geophysical data were acquired in <30-second cycles after which the IMU was returned to its initial position. Each data collection event consists of the following steps; initial ZUPT, acquire data, final ZUPT. During the initial ZUPT, the SAINT unit is set down on the tripod mount and remains stationary for 15 seconds. During data collection, the operator picks up the unit and acquires geophysical data for 30 seconds or less of free navigation over the area of interest. The data collection event ends when the SAINT unit is returned to its original location on the tripod mount for about 15-seconds final ZUPT.

Lights and audible signals aid the user for proper operation. During the 30 second free navigation period, various audible chirps are sounded with 10, 5, and 0 seconds remaining before a new ZUPT is required. Data density can be increased by resurveying any given anomaly.

6.4 CALIBRATION ACTIVITIES

Spatial measurements were made to record the three-dimensional position offset of the center of sensitivity of the EM61HH, which is defined to be the physical center of mass

of the figure-eight coil configuration, with respect to the IMU in the measurement frame of the IMU.

Daily calibration efforts consisted of collecting cued EM61HH data over a standard object. The data were collected using the same procedures as used over training and blind targets. The daily variations in the system response were monitored and remained within 10% of the reference values.

6.5 DATA COLLECTION

6.5.1 Scale of the Demonstration

The demonstration was conducted at the calibration and blind grids of the APG Standardized UXO Test Site.

6.6 SAMPLE DENSITY

EM61HH data spacing using the grid template is fixed at 15 cm in both directions. The choice of grid spacing was based on results of simulations of data inversion sensitivity as well as past experience and was concluded to be a good compromise of sample density and data collection time.

The EM61HH data spacing using the SAINT depends on the speed the operator moves the sensor over the target. Since sensor data is collected at discrete time intervals, desired sensor data density along the path over which the sensor is swept can be obtained by regulating the speed at which the sensor is swept. Free navigation is limited to 30 seconds to minimize positioning error. To cover a larger area than can be swept in 30 seconds, two or more data sweeps must be performed in series (separated by a ZUPT). A sample sweep pattern is shown in Figure 6-2. Since the ZUPT locations are the same, no special operation has to be performed in the post-processing software to overlay the adjacent collections. Anomalies that cover a large spatial area will typically have a lower data density than anomalies with a small spatial area.

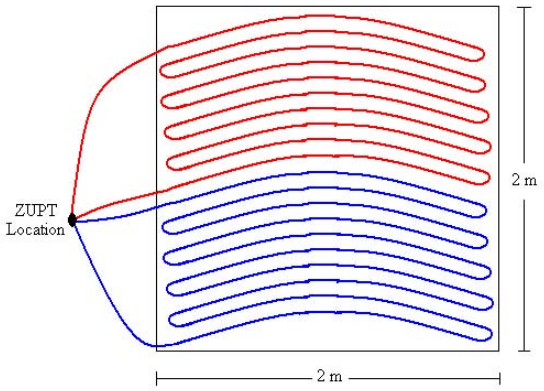

Figure 6-2: Sample sweep pattern to cover a 2x2m square area in two passes.

6.6.1 Quality Checks

For the grid template data, all QC checks and processing was done using IDL routines that were developed and refined during past surveys. The initial QC checks consisted of reading the data files, splitting them into grids, verifying that each grid has the correct number of marked data segments (36 grid points plus starting and ending background), and making raster plots of the data. Additional QC checks and processing will be done using routines that extract the background and grid point readings identified by event marks, allow display and editing of the data and characterize the anomaly. The anomalies were characterized by inverting the data to a dipole model each day, in order to monitor the fit quality, which is a measure of how accurately the modeled data matches the measured data. We have seen in past surveys that the fit quality decreases when measurement errors increase. The most common measurement error is positional error caused by the field crew not ensuring the crosshairs on the guide are aligned with the gridlines on the template.

Similar to the grid template data, the SAINT data were checked by monitoring the fit quality output from the inversion algorithms. The fit quality decreases with both low SNR signals and with poor positioning.

Any data set which was deemed unsatisfactory by the data analyst was flagged and not processed further. The anomaly corresponding to the flagged data was logged for future re-acquisition.

6.6.2 Data Handling

EM61HH data using the grid template are stored electronically as collected on the Allegro data acquisition computer and downloaded via serial port to a notebook computer for QC/analysis using Geonics supplied software. EM61HH data positioned using the SAINT are also stored electronically as collected on the SAINT acquisition computer and downloaded to a notebook computer using a USB or Ethernet cable. The SAINT acquisition computer is treated as another drive when connected to another computer and data is transferred using standard drag and drop methods.

Raw data and analysis results were backed up from the data analyst's computer to flash cards daily. These results were archived on an internal file server at SAIC at the end of the survey.

6.7 VALIDATION

With the exception of the Calibration Grid, the ground truth for the Standardized sites is held back from individual technology demonstrators to preserve the utility of the Blind Grid and Open Field Areas. Analysis results (i.e., prioritized dig lists) from the Blind Grid were submitted to ATC and the program office for performance evaluation.

7.0 DATA ANALYSIS AND PRODUCTS

7.1 PREPROCESSING

The data files for the grid template data nominally contain data for one or more targets. Different targets are identified by the survey line numbers in the file. In the data section following the survey line header, column 1 is an event marker which identifies readings at the grid locations over the target. The symbol "P" is the event marker when the sensor coil is over a grid location. The symbol "E" is the event marker when the sensor coil is being moved to the next grid location. Each survey line should have 38 data sequences with event marks. The first and last sequences are background readings taken in the air out of ground effects. The middle 36 correspond to locations on the 36 point measurement grid. Each of the 38 data sequences contain multiple readings when the sensor is stationary. The stationary readings are averaged and assigned a local XY location based on its fixed position on the grid template. The data for each 6x6 point data grid are then leveled using the before and after backgrounds.

The preprocessing for the SAINT exploits the operational requirement that the start and stop locations of the SAINT hardware be identical. The operator can free navigate for up to 30 seconds, at which time the unit must be returned to the same place it started. A tripod is used to simplify the return of the hardware to the identical location. Upon completion of the ZUPT, a blue indicator light illuminates on the SAINT enclosure signifying the operator can free-navigate when ready.

The post-processing software includes a GUI that requires the user to select the filenames for processing and the periods to process. The processing consists of the following components:

1 A pre-filter for detection of ZUPT intervals
2 Navigation equations and a Kalman filter [8]
3 Rauch-Tung-Streibel (R-T-S) Smoother
4 A component to translate the IMU position & attitude to the geophysical sensor based on the static 3-D position & orientation offset vectors
5 A component to interpolate the sensor position & attitude (recorded at up to 600 Hz) to the recorded EM61 times (recorded at approximately 15 Hz)

The error-state Kalman filter feeds corrections back into the navigation equations for both navigation errors and IMU sensor errors to optimally estimate the position and orientation of the IMU. The accuracy of these corrections is primarily a function of the quality of the IMU, the quality of the aiding measurements to the IMU and the quality of the model defining the IMU in the Kalman filter. The accuracy of the reported errors is primarily a function of the quality of the model defining the IMU. Since the IMU contains six sensors, and each has errors from bias, drift, alignment, scale factor, nonlinearity, asymmetry, and other sources, more than 50 states in the Kalman Filter were necessary to optimally model the IMU. The Kalman filter provides an optimal estimate of position based on all measurements available until time t_k. However, additional information contained in the measurements after t_k can further improve the estimate of position. An R-T-S Smoother [9] was implemented to compute an optimal smoothed path estimate

utilizing all available measurements within the data set.

In addition to the position and attitude estimates, the error estimates are provided for each of the components of position and attitude. Processing software outputs positions in a relative coordinate system with the origin at the ZUPT location and the orientation constrained by the compass.

7.2 TARGET SELECTION FOR DETECTION

All targets within the calibration and blind grids were surveyed.

7.3 PARAMETER ESTIMATION

The EM61HH data are inverted using the standard induced dipole response model wherein the effect of eddy currents set up in the target by the primary field is represented by a set of three orthogonal magnetic dipoles at the target location [10]. The measured signal is a linear function of the induced dipole moment **m**, which can be expressed in terms of a time dependent polarizability tensor **B** as

$$\mathbf{m} = \mathbf{U}\mathbf{B}\mathbf{U}^{T}\cdot\mathbf{H}_0$$

where **U** is the transformation matrix between the physical coordinate directions and the principal axes of the target and $\mathbf{H}_0$ is the primary field strength at the target. The eigenvalues $\beta_i(t)$ of the polarizability tensor are the principal axis polarizabilities.

Given a set of measurements of the target response with varying geometries or "look angles" at the target, the data can be inverted to determine the (X, Y, Z) location of the target, the orientation of its principal axes (ψ, θ, ϕ), and the principal axis polarizabilities (β_1, β_2, β_3). The basic idea is to search out the set of nine parameters (X, Y, Z, ψ, θ, ϕ, β_1, β_2, β_3) that minimizes the difference between the measured responses and those calculated using the dipole response model.

In some situations (depending on target size, orientation and distance from the sensor head) there is a bit of ambiguity regarding the "correct" values of the β's and the depth. We suspect that this is due to failure of the dipole response model to faithfully reproduce the signal when the dimensions of the target are comparable to distances over which there are significant changes in the primary field (and the reciprocal received field). For most UXO, there is one large β corresponding to the axial response and two smaller, equal β's corresponding to transverse responses. With ordnance items on a test stand, we find that the depth at which the secondary β's are equal is not always the depth that minimizes the RMS deviation between the data and the dipole model. Consequently for the grid template, the EM data were processed by "focusing" the measurement array at depths from ~5 cm to 100 cm below the ground level. As a function of focus depth, we fit the array data to a dipole response model using a least squares procedure. We then looked at the best fit eigenvalues and residual error as functions of depth to find the "correct" values of the β's and the depth.

There are several additional complications in inverting the EM61HH/SAINT data. The first is the added requirement for modeling the sensor's dynamic time response. The receiver output of this sensor is analog integrated with a filter that both shifts and distorts the sensor's response. This filter was added to the forward model used by the inversion algorithm. The second complication is the sensor bias drift. Over minutes of data collection, the zero level of the sensor changes. The data collected here starts with the sensor on a metal tripod with an unknown offset. It then moves back and forth over an object perhaps reaching zero at points, perhaps not. Because of this, an offset parameter has been added to the data inversion process.

7.4 CLASSIFIER AND TRAINING

As part of this demonstration and under previous project we have collected in-air data for many of the standard APG ordnance targets. We also collected additional in-air training data for any ordnance not already in our library. The combination of these data was used for the fit library entries. Many of the targets are composites of two or more distinct parts, like a steel body combined with an aluminum tail assembly. Depending on the distance between the sensors and the target, such items can exhibit a range of slightly different EMI signatures corresponding to excitation from different directions. We included measurements with the target oriented nose up, nose down, flat and obliquely relative to the sensor.

Our experience at our Blossom Point test site has been that polarizabilities determined from in-air measurements are indistinguishable from those determined from measurements taken over buried targets. We used data from the calibration lanes, which contain several instances of each target, to establish that this holds true at APG.

We used target features for clutter items found in the calibration grid. Unfortunately there were only eight clutter items in the calibration grid so we augmented our clutter library with features derived from previous surveys over APG. In particular, we used the results from the ESTCP project 200108 which demonstrated the discrimination capabilities of the EM61HH-MK2 over the blind grid.

Target classification was based on a library matching procedure. We compare the quality of an unconstrained dipole inversion of the EM61HH-MK2 data to the quality of a dipole fit constrained by principal axis polarizabilities drawn from the signature library. The library values were based on the mean of the log of the best unconstrained fits from the training data. Fit quality is the squared correlation coefficient between the model fit and the data. If the ratio of the constrained fit quality to the unconstrained fit quality (ρ) is one, then the library item is as good a match to the data as possible. If the ratio is small, then the library item is a poor match.

Rule based decisions that incorporate the fit ratio, polarizability coefficients, signal amplitude and fit error were used to make the final classification decision. The thresholds were decided by inspection of the above parameters calculated from the training data.

7.5 DATA PRODUCTS

We utilized the standard reporting templates for the Blind Grid (Figure 7-1).

BLIND TEST GRID									
	Letter	Number	Response Stage	Discrimination Stage/Ranking	Classification (Use B for Blank)	TYPE	Depth (M)	Azimuth (Degrees)	Dip (Degress)
1	A	1	959.5	0.9852	O	37mm	0.19	-6.0	18.9
2	A	2	1.0		B				
3	A	3	1.0		B				
4	A	4	1.0		B				
5	A	5	1633.2	0.9821	O	37mm	0.11	61.7	9.8

Figure 7-1: APG Blind Grid report.

8.0 PERFORMANCE ASSESMENT

APG Demonstration

Overview

The SAINT system was demonstrated on the APG Calibration Grid and Blind Grid from June 22nd to July 8th, 2010. A total of 12 days was spent on site. The first day was spent flagging the Blind grid and the last day packing up. The data was collected by NAEVA Geophysics field personnel. The field operators were trained on the SAINT for one day prior to the test; they were already familiar with the EM61-HH and its operation with the Allegro.

Data collection was carried out by two field workers; one to collect data and the other to take notes and assist as needed. An analyst was on site for half of the time to quality check the data as it was collected. After that, the data was transferred nightly to an analyst off site for processing. Typically, data would be downloaded from the SAINT twice daily, at lunch and the end of the day. Batteries would be swapped then as well.

The only major problem encountered was a loose cable. Operations had to be shut down for ½ day to return the equipment to ENSCO to repair the cable and check the system out. Besides this, every 10 or 20 data files, a glitch would occur in the raw data files. A way was found to step past the corrupted data and process the rest of the file. Part of one afternoon was lost to a thunderstorm.

All 66 cells in the Calibration Grid were measured by the SAINT. On the Blind Grid, the EM61-HH was swept over the cell area. If no measurable signal (~ 10 mV) was noted by the operator, the cell was recorded as empty and no SAINT data was collected. On average, 50 to 100 cells were measured per day.

Template Comparison

As a baseline comparison, the Calibration and Blind Grids were also measured with the EM61-HH placed on a wooden template grid. Photos of both the template and SAINT measurements being made at APG are shown in Figure 8-1. The template consisted of a 6 by 6 square grid of points with a spacing of 0.15 m. Each grid had 38 measurements with the first and last being in the air to zero the sensor. Template measurements took roughly 3-4 minutes a cell with a comparable average daily rate to the SAINT. Logistically, the wooden template had to be moved cell to cell which was comparable to moving the SAINT tripod cell to cell. Approximately, 10 grids were re-measured due to operator error in taking the data (grid points skipped or repeated). Both the SAINT and template data were fit with the same EMI model. Discrimination was based on the same library fit and ratio test. Cells that were noted empty for the SAINT were not measured by the template. Separate target reports were generated and handed in for grading with both approaches. As with the SAINT, a set of data quality and fit quality plots were generated for each cell. Examples of these are shown in Appendix B and C.

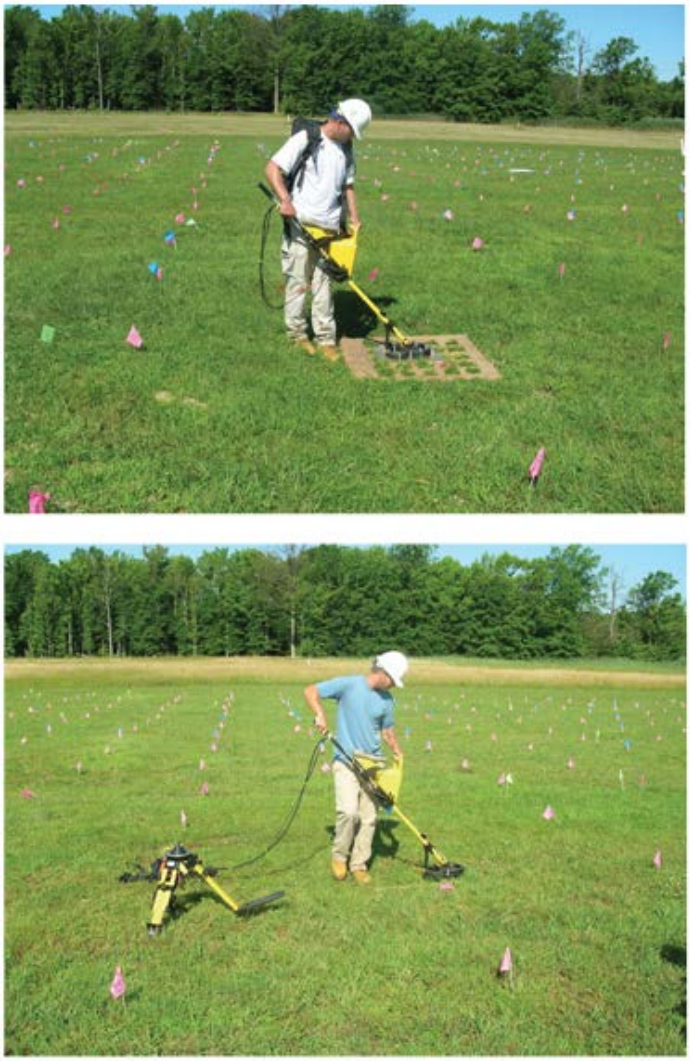

Figure 8-1 Photographs of the EM61HH plus template positioning system (top photo) and SAINT positioning system (bottom photo)

Results

The plots in Figure 8-2 are a basic comparison of the EM61-HH data collected with the template and the SAINT. The left side is template data, and the right side is SAINT data. Both were collected over the same object on the Blind Grid. The top plots are contours of the data and the bottom plots are the data as sampled over time. The contoured template data has symbols plotted at each measurement point. The contoured SAINT data has a dotted line indicating the sensor trajectory. The SAINT data has been time shifted to account for the sensor's analog filter. The template data is not affected by the filter because it is collected with the sensor stationary at each point. The filter also stretches and damps the signal which is why the SAINT signature is different from the template signature. The signature shown is typical of small, shallow clutter measured by the EM61-HH. Because the transmit/receive coils are not co-located, there is a region where the signal actually goes negative. With six continuous slices of data instead of six sets of

six points, the SAINT trajectory collects a higher density of data points and better resolves the signature. The trade-off is larger errors in positioning. The red curves in the bottom plots are the modeled fits to the data.

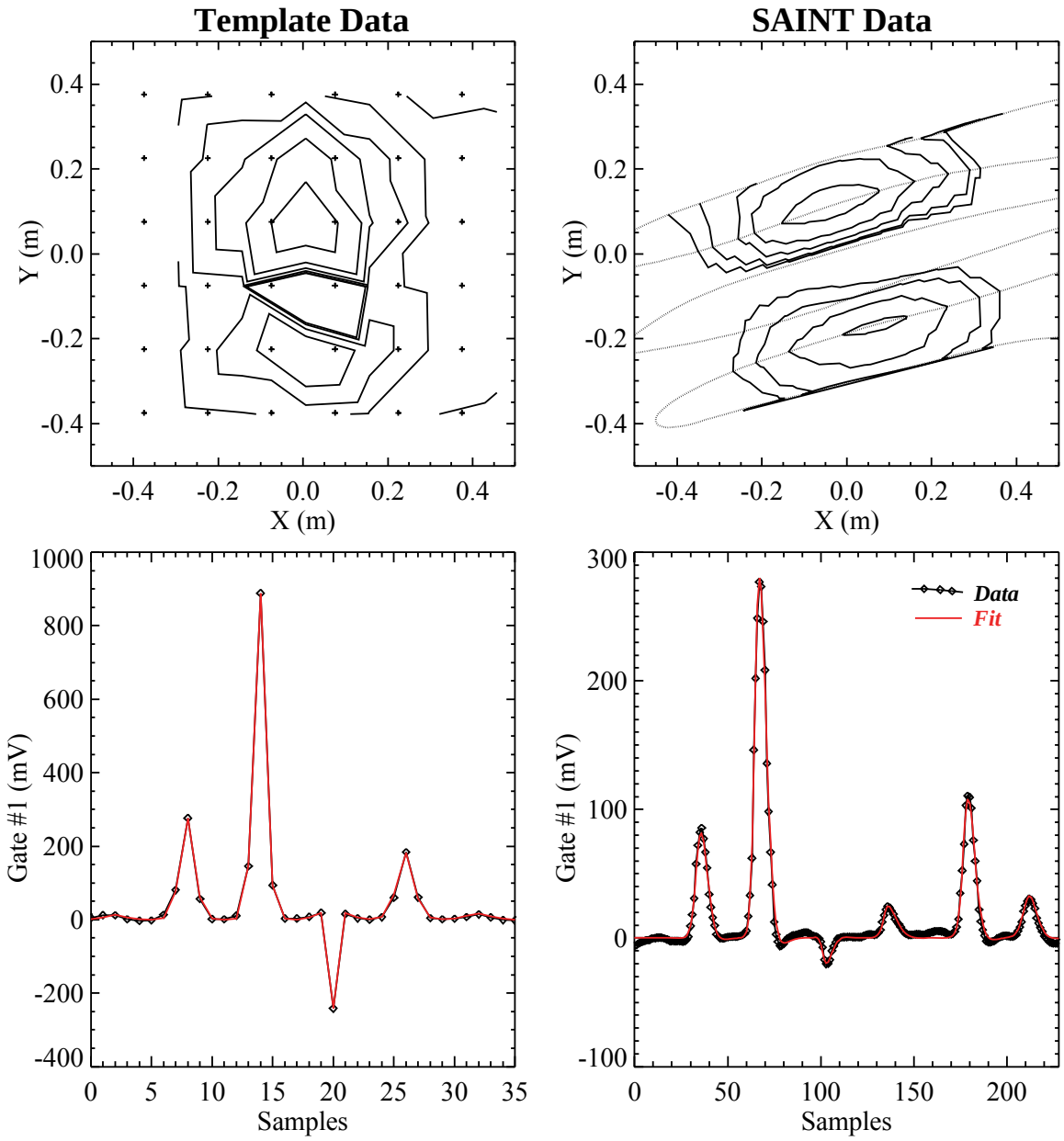

Figure 8-2 Representative data acquired using a template (left panels) and SAINT (right panels). Note the increased data density acquired by the SAINT system.

An unexpected outcome of EM61-HH measurements on the Calibration Lanes and Blind Grid at APG was the large amount of very small, shallow clutter detected. Both sets of measurements were taken close to the surface (< 10 cm). Combined with the small coils of the EM61-HH, small bits of shallow metal produce very large signals. Figure 8-3 is an example of this on the Calibration Lanes. The top plot is a contour of the data in black

with the SAINT trajectory in red. The bottom plot is the signal in black as function of samples collected over time. There is a broad, low amplitude signal from the ordnance item buried here and a large spike off to the left from a clutter item. In this case, the clutter data could be weighted out of the inversion process and a reasonable fit to the ordnance signature achieved. This model fit is plotted in red on the bottom plot. In many cases, this was not the case and the item would be categorized as "Can Not Analyze." With the higher density of data, it was easier to resolve these clutter situations with the SAINT data set, but many clutter spikes were noted with the template set as well. In either case, the EM61-HH probably detected these clutter items on some cells that the ground truth for the site considers to be empty cells. Since this is not a detection test, but a discrimination study, we were not concerned with this in our analysis of the data. Anecdotally, the small clutter is apparently the result of bringing in fill dirt that was thought to be clean, but turned out not to be.

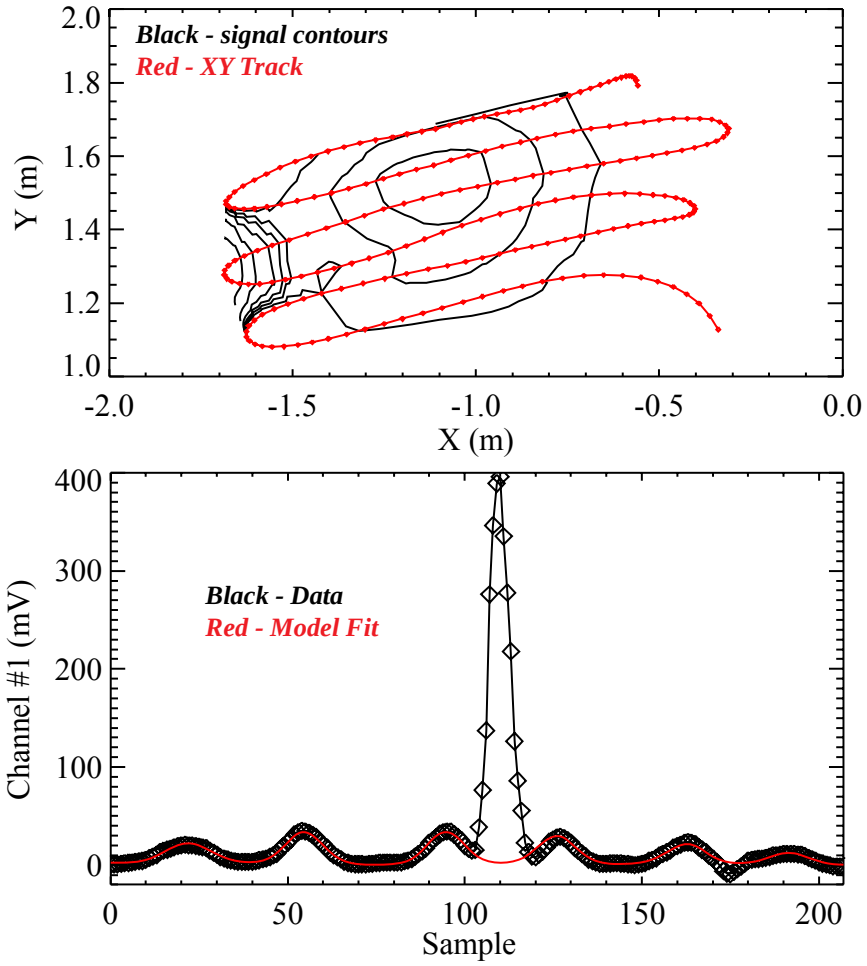

Figure 8-3 SAINT positioned data showing a high amplitude anomaly (-1.5m X top and ~110 samples bottom) that is superimposed onto the broader, lower amplitude signature of the test target.

Separate target reports were handed in for the SAINT and template data sets. For the standardized test sites, the target report is divided into a detection based "response stage" ranking and a "discrimination stage" ranking. For the response stage, the EM61-HH was manually swept over the center of each cell. If there was no measurable signal (~ 10 mV) within roughly 0.25 m of the cell center, the cell was determined to be empty for both data sets and no further measurements were taken. The search was limited to the center of each cell, because (as discussed above) there was a lot of small clutter found over the site. The response stage factor was set to 1.0 for empty cells and to the peak measured signal (first time gate) on cells that were not. For "classification", the empty cells are labeled "B" for blank. All of the SAINT and template data with measurable signal was run through the dipole model based inversion and a standard set of diagnostic plots generated for each cell (see appendices B and C). As discussed earlier, the data was inverted with no constraint on the magnetic polarizations and then inverted with the polarizations constrained to a library set of values for the expected ordnance set. The ratio of the fit error (constrained over unconstrained) was used as the discrimination stage ranking factor and the library entry that best matched was used to declare the ordnance type in the target report. This discrimination ranking factor varied from 0.53 to 0.9998 for reasonable data sets. Based on pre-test data, Calibration Lane data, and general observation over the Blind Grid data, a threshold of 0.98 was empirically selected as the threshold between declaring the "classification" category as "C" for most likely clutter or "O" for most likely ordnance. Lastly, the diagnostic plots were looked through by the analyst for any problems. Cells where there were weak signals, multiple objects, or otherwise poor fits were labeled as "Can Not Analyze." The standardized target reports do not account for this category. On an actual site, one would have to dig these items because the analysis could not identify them with certainty. In this spirit, the discrimination stage ranking factor for these items was simply set to 1.0. They are all ranked first to dig in no particular order. There were 44 of these items in the SAINT target report and 41 in the template target report.

The two target reports for the APG Blind Grid were submitted for grading and the returned results are presented in Appendix D. An overall synopsis is shown in Table 8-1 thru Table 8-5 with a comparison to the performance of the advanced 5x5 TEM array (MR-0601) on the same site.

Table 8-1 presents the detection results of the EM61-HH (same for SAINT and template) and Table 8-2 presents the TEM array detection. The probability of detection, P_d, is broken down into three ordnance categories (105mm's, 60mm/81mm, and 25mm/37mm) as well as three depth ranges by ordnance diameter. The EM61-HH missed only 105mm's (projectile and HEAT) and only at their deepest depth range (8-12 times their diameter) with a P_d of 0.67 in this range. All other P_d's were 1.0 with an overall P_d of 0.99. With the small coils of the EM61-HH this result was expected. In comparison, the 5x5 TEM array missed fewer of the deep 105mm's with a P_d of 0.83 in this category. With larger coils and stationary data collection, the detection of the 5x5 TEM array is expected to be better for deeper ordnance items.

Table 8-1. EM61-HH Response Stage P_d's

	All Types	105-mm	81/60-mm	37/25-mm
	0.99	0.98	1.00	1.00
By Depth				
0 to 4D	1.00	1.00	1.00	1.00
4D to 8D	1.00	1.00	1.00	1.00
8D to 12D	0.67	0.67	0.00	1.00

Table 8-2. TEM Array Response Stage P_d's

	All Types	105-mm	81/60-mm	37/25-mm
	0.99	1.00	1.00	1.00
By Depth				
0 to 4D	1.00	1.00	1.00	1.00
4D to 8D	1.00	1.00	1.00	1.00
8D to 12D	0.78	0.83	0.00	1.00

Table 8-3 presents the discrimination stage P_d's of the three systems. At their designated discrimination stage thresholds, the SAINT results are equal to the TEM results with a P_d of 0.99. The template data and SAINT data were processed with the same discrimination algorithm (library ratio test) with the same threshold setting, but the template data only achieved an overall P_d of 0.93. Table 8-4 compares other general statistics between the systems. The second column is efficiency which is a measure of how much of the ordnance detected was identified as ordnance in the discrimination stage. In this column, the first number is the efficiency at the operator's threshold and the second is the highest efficiency achieved at a lower threshold level ("without loss of P_d"). At the operator's threshold with an efficiency of 1.0, the SAINT system identified all detected ordnance as being ordnance. The TEM efficiency is 0.99, but achieves 1.0 at only a slightly lower threshold. The template efficiency is 0.92 at the threshold, but achieved 1.0 at a lower threshold setting. Between discrimination stage P_d and efficiencies, these results indicate that all three systems can identify ordnance given a correct setting of the operator's threshold.

Table 8-3**.** Comparison of Discrimination Stage P_d's

Data Set	All Types	105-mm	81/60-mm	37/25-mm
Template	0.93	0.94	0.94	0.98
SAINT	0.99	0.98	1.00	1.00
5x5 TEM Array	0.99	0.98	1.00	1.00

Table 8-4**.** Comparison of Overall Statistics

	Efficiency	P_{cd}	P_{ba} *Response Stage*	P_{fp}	False Positive Rejection Rate	P_{ba} *Discrimination Stage*	Background Alarm Rejection Rate
Template	0.92/1.0	1.0	0.42	0.35	0.71/0.31	0.14	0.66/0.60
SAINT	1.0/1.0	1.0	0.42	0.43	0.63/0.63	0.16	0.63/0.63
5x5 TEM Array	0.99/1.0	0.90	0.12	0.03	0.99/0.95	0.05	0.61/0.57

In terms of detecting clutter, the EM61-HH outperforms the TEM array. This is most likely the indication of small metallic clutter present on the Blind Grid as already mentioned. In terms of emplaced clutter, the EM61-HH detected all of it with a P_{cd} of 1.0. The TEM array P_{cd} is 0.90. On "Blank" cells (no emplaced clutter or ordnance), the EM61-HH has a response stage probability of "background alarm", P_{ba}, of 0.42 versus the TEM result of 0.12. The EM61-HH P_{ba} is probably a good indication of how much small metallic debris there is.

In terms of rejecting clutter at the discrimination stage, the TEM array outperforms the SAINT and template systems. At the operator's threshold, the SAINT data resulted in a probability of false positive, P_{fp}, of 0.43 and the template data gave 0.35. The TEM array P_{fp} is 0.03. The false positive rejection rate, a measure of how much detected, emplaced clutter is identified as clutter, is 0.71 for the template and 0.63 for the SAINT data. Again, at the template threshold for a P_d of 1.0, the rate is 0.31 compared to the SAINT's rate of 0.63. The SAINT data is significantly better at rejecting emplaced clutter. The TEM array outperforms both with a rejection rate of 0.95 at a P_d of 1.0. For the background alarm rejection, all systems performed comparably (~ 0.60), but the TEM detected far fewer of the small clutter items on the empty cells.

Table 8-5 presents the number of emplaced ordnance items correctly identified by type. This number is at the operator's threshold. Ordnance not detected is included in the total count. For small ordnance (25mm/37mm), the SAINT correctly identified 100% and the

template only 93%. The numbers decrease for the two larger ordnance categories (97% and 77% for the SAINT). The TEM array numbers are listed individually, but are actually comparable to the SAINT performance. It should be noted that the EM61-HH library grouped both types of 105mm's together. The TEM array, with its later time gates, could distinguish between the two items.

Table 8-5**.** Comparison of Correct Type Classification

	25mm/37mm	**60mm/81mm**	**105mm's**	**Overall**
Template	93%	87%	73%	84%
SAINT	100%	97%	77%	91%
5x5 TEM Array	100/100	100/93	70/67	?

To better understand these results, we compared the exact target reports of the template, SAINT, and TEM array for the Blind Grid. To analyze the template and SAINT results, we simply used the TEM array data as ground truth. Overall, the TEM array missed or was wrong on only a small number of items. Rather than separate clutter into emplaced and background alarms, we considered both as just one set of clutter. Lastly, we considered the category of "Can't Analyze" separately. Figure 8-4 presents a discrimination stage ROC curve based on this work. The x-axis is just a straight count of clutter items. If the SAINT data set or template data set detected a signal on a non-ordnance cell, it is counted as a valid clutter count, even if the TEM detected nothing on that cell. The y-axis is a percentage of the total ordnance based on what the TEM identified as ordnance. The black curve is from the SAINT set and the red curve is the template set. Items in the "Can't Analyze" category have been ranked first in the ROC curve (all were fixed with a library ratio of 1.0), but plotted on the negative y-axis. Both the SAINT and template data had comparable numbers in this category (44 and 41) and roughly the same percentage of ordnance occurred here (about 5%). While both ROC curves rise rapidly, the SAINT reaches a P_d of 1.0 with about 20 fewer false alarms. Ignoring the "Can't Analyze" items, the SAINT rejects about 75% (120/160) of the clutter items at this point. The template data rejects about 63% of the clutter at its 1.0 P_d point.

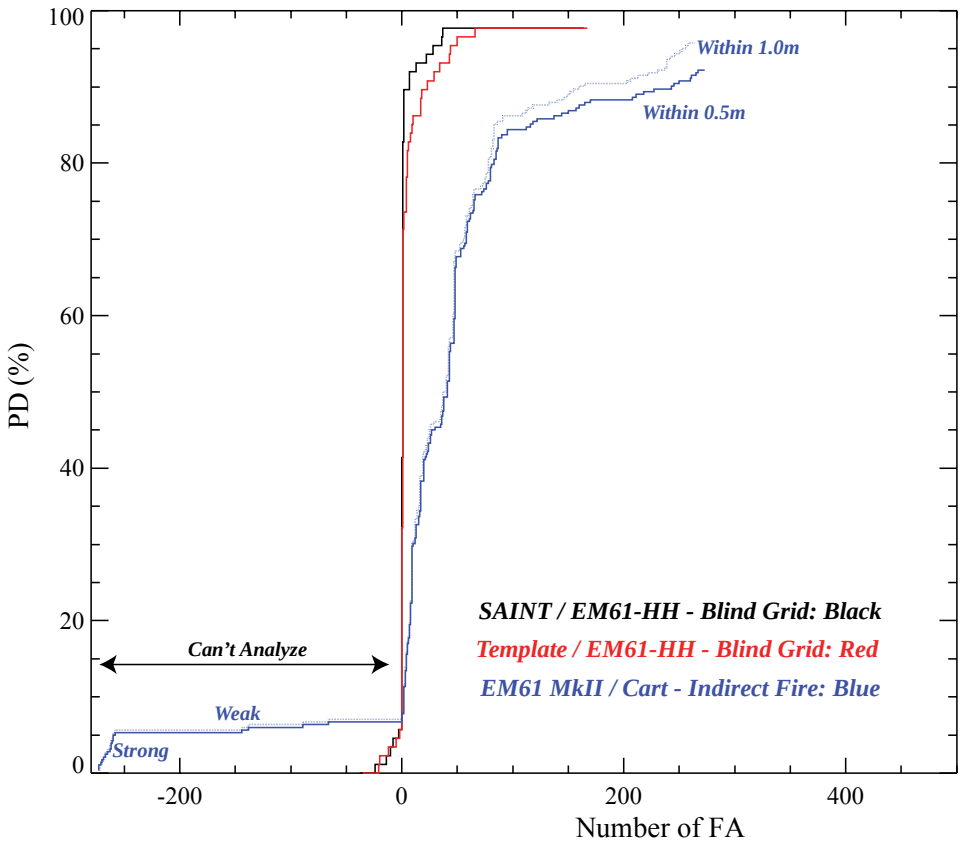

Figure 8-4 Receiver operating characteristic (ROC) curve comparing classification performance between SAINT+EM61HH, Template+EM61HH, and an EM61 MkII sensor.

The TEM array collected data on the Indirect Fire site at APG. For comparison, a standard EM61 MkII cart system was deployed and analyzed over the same field [REF 7]. In a fashion similar to the SAINT/template on the Blind Grid, we considered the TEM array results as ground truth and created the blue ROC curve in Figure 8-4 for the EM61 cart results. While not a direct comparison, it does indicate that the EM61-HH positioned either by the SAINT or the template performs significantly better than standard EM61 MkII data on a survey cart with GPS positioning.

Figure 8-5 and Figure 8-6 plot the inverted polarizations for the items that the TEM array definitely identified as ordnance. The polarizations are from the first time gate. The x-axis indicates the primary polarization. The y-axis plots the second and third values connected by a vertical line and a symbol at their average. The top plots in Figure 5 are from the EM61 Cart on the Indirect Fire field. The middle plots are from the template data on the Blind Grid. The bottom plots are from the SAINT data on the Blind Grid. The three large ordnance types are shown: 60mm on left, 81mm in middle, and 105mm on right. The red circles are centered on the library polarization values. The EM61 Cart plots clearly show that this data cannot be used to accurately invert the three polarizations. Between the data sparseness (0.75 m track spacing) and the positioning errors (GPS RMS error ~ 2-3 cm), one can at best use the primary polarization as an indication of size (or

the sum of the polarizations squared). Even looking at only the primary polarization, there is considerable overlap between the three ordnance types. Overall, the template and the SAINT data show very tight clustering of the polarizations. The three ordnance types can be clearly distinguished with a single time gate. The template data shows some extra spread for the 105mm fits. The SAINT has several individual outliers for the 60mm and 105mm. The 81mm outliers in both data sets are clustered and based on TEM analysis are from a different type of 81mm mortar buried on the Blind Grid. Figure 8-6 shows the inverted polarizations from SAINT and template data over the smaller items: 25mm and 37mm. There are no EM61 Cart results for these small items, because they are not present on the Indirect Fire site. For the small ordnance, both data sets are tightly clustered and there is no uncertainty as to the ordnance type. Figure 8-7 plots the SAINT polarizations of items that the TEM data indicates are clutter, but that the "library ratio test" processing of the SAINT data flags as ordnance (false positives). Many of these false positives are from small clutter items with polarizations about the 37mm library value. Given the spread of these clutter polarizations relative to the actual 37mm polarizations, the "library ratio test" may be too conservative of an approach for discriminating the inversion results of SAINT data. It may actually be worth comparing the polarization values.

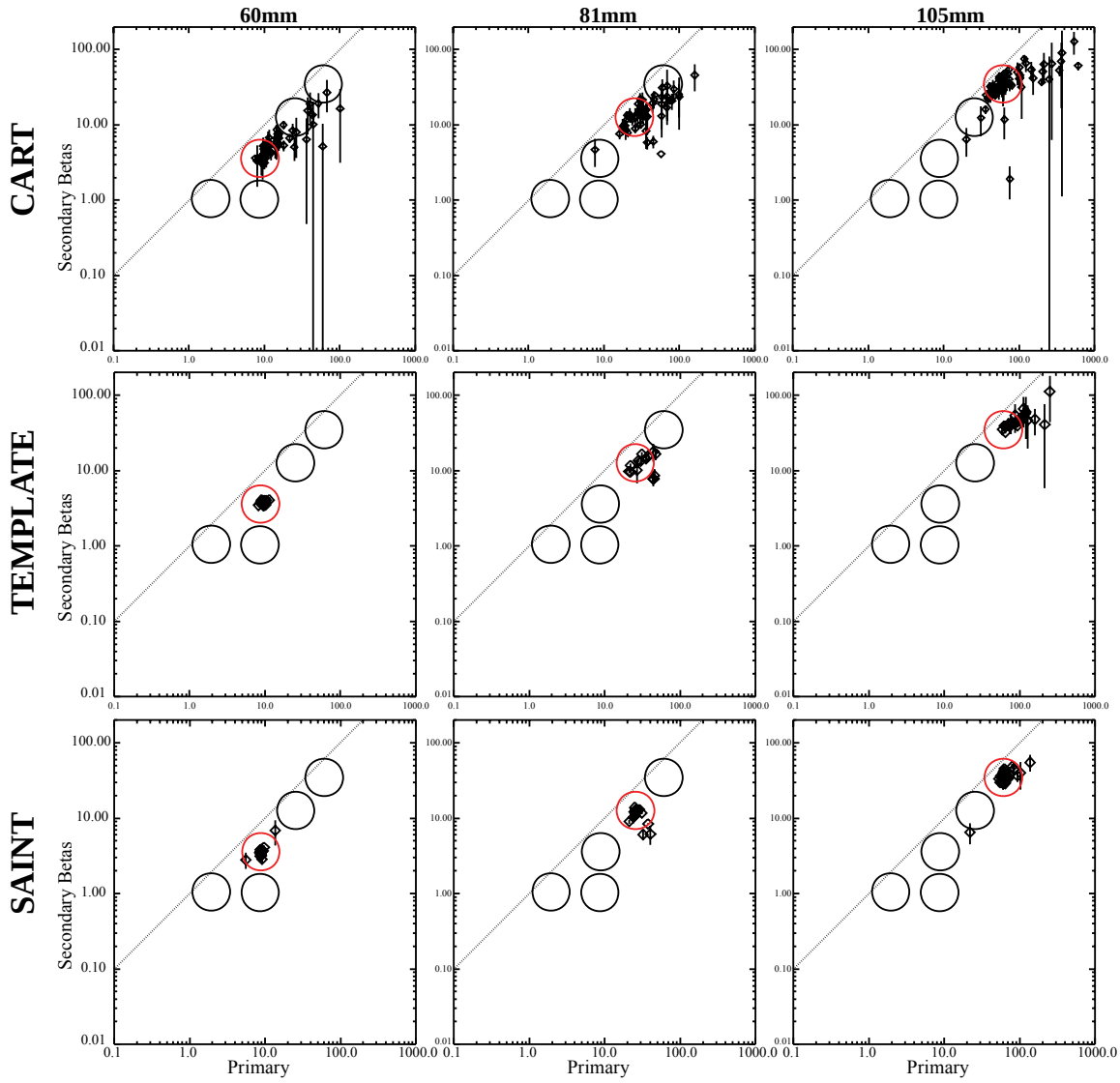

Figure 8-5 Principal axis polarizations for anomalies that were declared as 60mm, 81mm, and 105mm by NRL's TEM sensor.

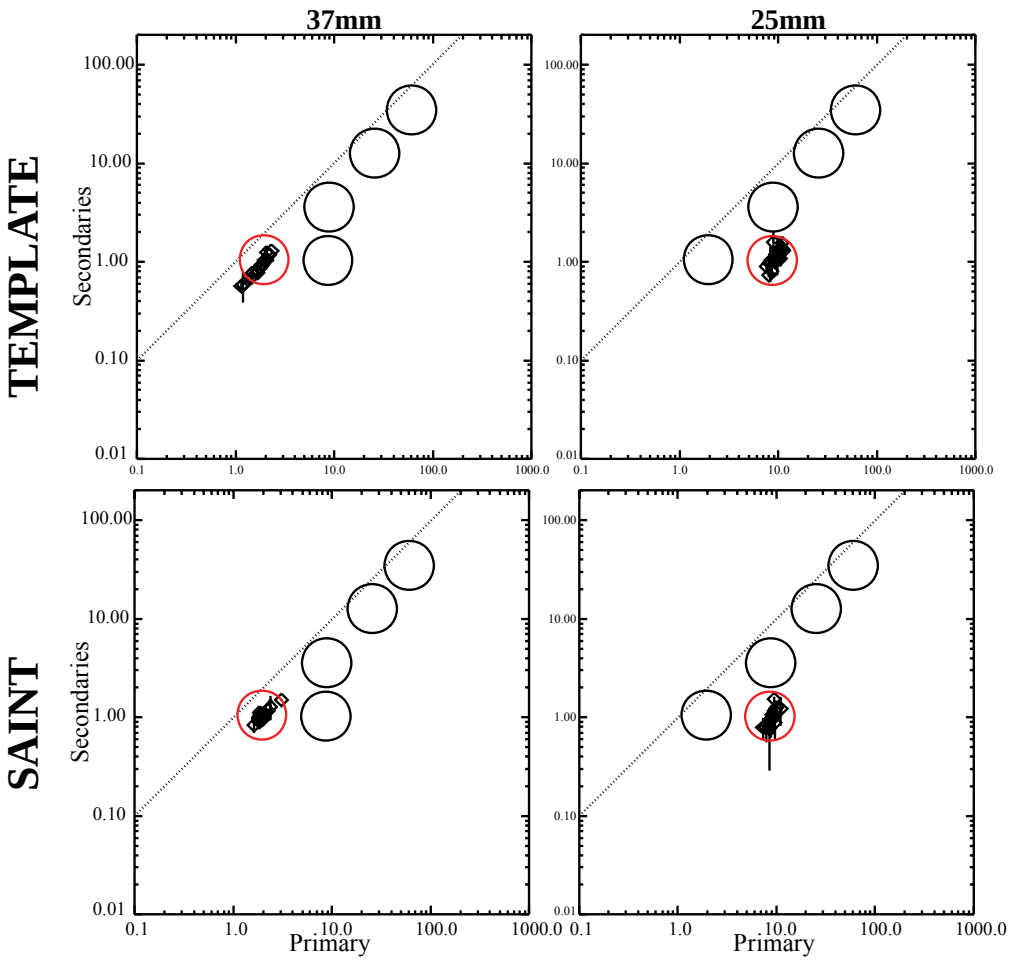

Figure 8-6 Principal axis polarizations for anomalies that were declared as 37mm and 25mm projectiles by NRL's TEM sensor.

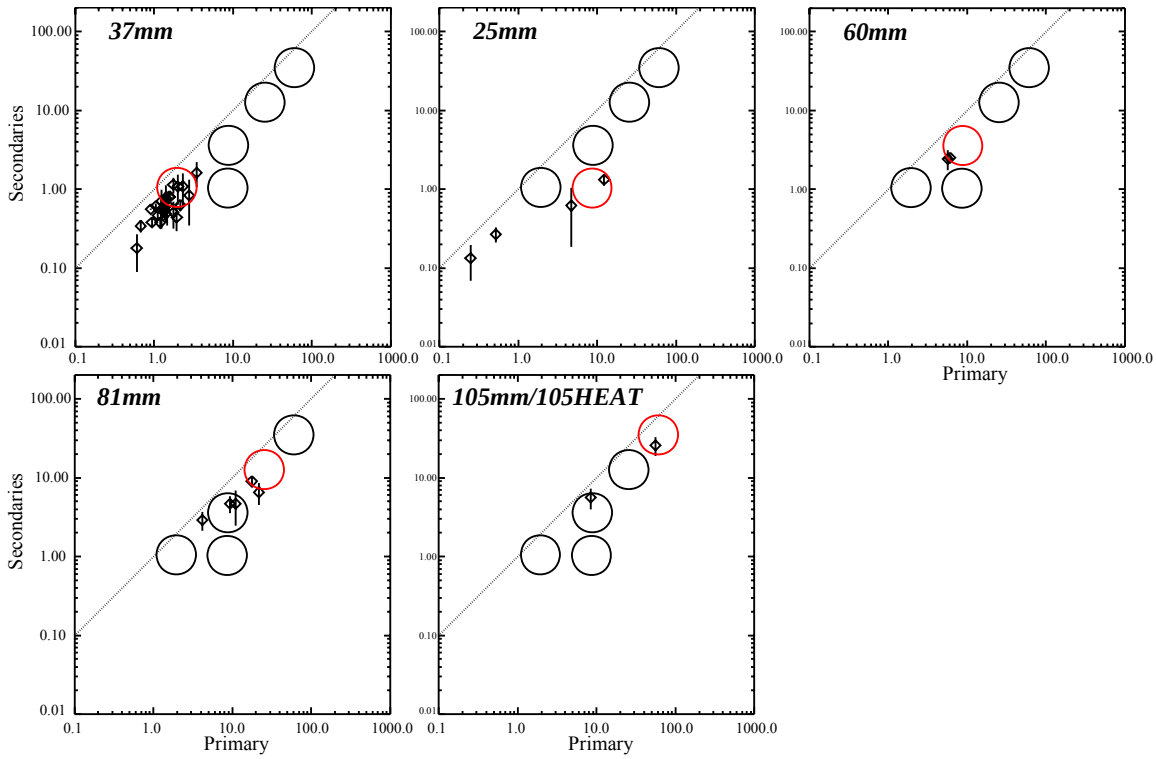

Figure 8-7 Principal axis polarizations for anomalies that were declared clutter by NRL's TEM sensor.

9.0 COST ASSESMENT

Table 9-1. Cost Elements.

Cost Element	Data to be Tracked	Estimated Costs
Instrument Cost	Component costs and integration costs • Engineering estimates based on current development • Spares and repairs	EM61HH - $20k SAINT - $60k Template - $20
Mobilization and demobilization	Cost to pack the equipment, mobilize to the site, and return • Derived from demonstration costs	$1k
Instrument set-up costs	Cost to assemble the system and perform initial calibration tests. • Personnel required • Hours required	$1k
Survey costs	Unit cost per anomaly investigated. This was calculated as daily survey costs divided by the number of anomalies investigated per day. • Daily warm-up and calibration • Survey personnel required • Survey hours per day • Daily equipment break-down and storage	$14
Discrimination data processing	Processing costs per anomaly • Personnel required • Time required per anomaly	$10

9.1 COST DRIVERS

The primary costs drivers are related to data collection (survey costs) and to data analyses. Survey costs were comparable for the template-based or SAINT-aided EM61HH systems. As demonstrated here, however, repeat data collects were performed for all blind targets to mitigate an unpredictable spike which occasionally occurred. Repeat data collects will not be needed after the sensor spike issue is resolved. Because both data were analyzed using the same inversion algorithms, the analysis costs were also comparable.

9.2 COST BENEFIT

The realized cost benefit for any given site depends greatly on the actual costs required for excavation. The SAINT+EM61HH system had discrimination Pd of 0.99 while rejecting 0.63 of the clutter. The template+EM61HH system was only slightly poorer. These results, if adopted and proven reliable going forward, would allow the stakeholder(s) to uniquely address suspect UXO while leaving over 60 percent of the objects in the ground.

10.0 IMPLEMENTATION ISSUES

We collected data with an EM61HH sensor using two different methods for spatially registration. The two methods included a simple template and the SAINT system. No significant problems or issues were noted by the field crew while acquiring either data set. Because of an irregular and unpredictable data spike associated with the SAINT positioning system, we acquired data at each target location multiple times. Although this approach maximized data quality because we could discard problematic data, it did slow down production. Aside from this, there were no implementation issues of note.

11.0 REFERENCES

1. "Report of the Defense Science Board Task Force on Unexploded Ordnance," December 2003, Office of the Under Secretary of Defense for Acquisition, Technology, and Logistics, Washington, D.C. 20301-3140, http://www.acq.osd.mil/dsb/uxo.pdf.

2. T. Furuya, T. Bell, and B. Ambrose, *Handheld Sensor for Unexploded Ordnance Discrimination*, SERDP/ESTCP Partners in Environmental Technology Symposium, 2002.

3. T. Bell, B. Barrow, and J. Miller, Subsurface Discrimination Using Electromagnetic Induction Sensors, IEEE Transactions on Geoscience and Remote Sensing, Vol. 39, no. 6, pages 1286-1293, June, 2001.

4. MM-0604, Small Area Inertial Navigation Tracking (SAINT) System for Precise Location of Buried UXO, Environmental Security Technology Certification Program, Final Report, January 2007.

5. T. Bell, N. Khadr, and B. Barrow, *Handheld UXO Sensor Improvements to Facilitate UXO/Clutter Discrimination*, SERDP Project MM-1381, Final Report Draft.

6. Aberdeen Proving Ground Soil Survey Report, October 1998.

7. Nelson, H. H. and Steinhurst, D. A., "MTADS Geophysical Survey of the ATC Standardized UXO Technology Demonstration Site Proposed Active Response Area," Naval Research Laboratory Letter Report Number 6110-089, August 6, 2003.

8. Rogers, R. M., *Applied Mathematics in Integrated Navigation Systems*, AIAA, 2000

9. Rauch, H.E., Tung, F. and Streibel, C.T. , "Maximum Likelihood Estimates of Linear Dynamic Systems", AIAA J, volume 3, No., 8, pp. 1445-1450, 1965.

10. Bell, T. H., Barrow, B. J., and Miller, J. T., "Subsurface Discrimination Using Electromagnetic Induction Sensors," IEEE Transactions on Geoscience and Remote Sensing, Vol. 39, No. 6, June 2001.

APPENDIX A: SYSTEM IMPROVEMENTS AND VALIDATION TESTS

The improved system is shown in Figure A-1. The system is enclosed in the triangular, ABS plastic case with handle that can be attached to an EMI sensor pole. The SAINT was again attached to an EM61-HH MkII, but options were kept open for attaching it to handheld systems under development. The case contains a single board computer (SBC), an electronic compass, and an IMU (Honeywell 1900). The EM61-HH is controlled by the standard Allegro handheld computer running software provided by Geonics. The combined instruments sit on an improved tripod stand.

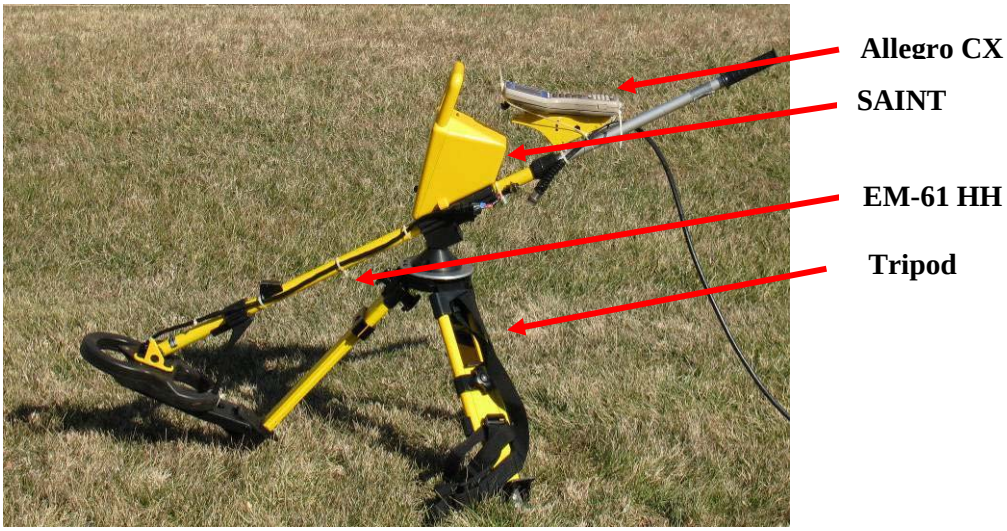

Figure A-1 The SAINT system installed on an EM-61 HH sensor

The IMU data collection was changed from a simple embedded processor to a single board computer. This was done to make the system more versatile. The SBC has a variety of digital input/output options (serial lines, USB ports, etc.). A serial line is used to provide synchronization of the IMU data with the EM61 data. The serial line grabs the trigger characters sent from the Allegro to the EM61 as well as the data packets sent back from the EM61 to the Allegro. Each set is time stamped with the count of the most recent IMU packet received. The IMU packets come in at a rate of 600 per second. The EM61 data is time stamped to within a small number of IMU counts (~3-5) and a timing accuracy of < 10 milliseconds. For other EMI systems, the various I/O lines could be used to time stamp other EMI data streams or to provide a timing pulse out to other EMI systems. The prototype system had no synchronization of the EMI and IMU data.

The IMU and EM61 data are stored in files on an SD memory card on the SBC. The data is moved to a PC computer for post-processing. To transfer the data files, the SBC has been set up to emulate a USB memory device. By switching the SAINT system to a USB cable, it plugs into a PC and automatically mounts as an external drive. The files can be dragged and dropped from the SAINT to the PC. The prototype system had a compact

flash card that had to be physically removed and plugged into a PC with a flash card reader.

Figure A-2 shows a close up of the SAINT case. There is a green LED push button for powering the system up, pausing data collection, and powering the system off. There are two status LED's on top of the case. The blue one provides status and timing flashes during data collection and file download. The red LED indicates system errors. Errors and timing are also indicated by an audible tone. Cabling for power, downloading data, serial lines, and the tripod switch attach to the side of the case. Further detail of cabling, operations, and LED status lights is given in the SAINT user manual [REF 5]. Figure A-3 shows the battery pack for the SAINT attached to the EM61 backpack. The new system is powered by a laptop style, lithium ion battery. It is capable of running the SAINT for over 8 hours. There is a spare battery and an easy to use charger. In the field, the battery was usually changed at the mid-day break to insure no possible loss of power. The battery pack has its own on/off button with a red LED to indicate that the battery pack is providing power to the SAINT.

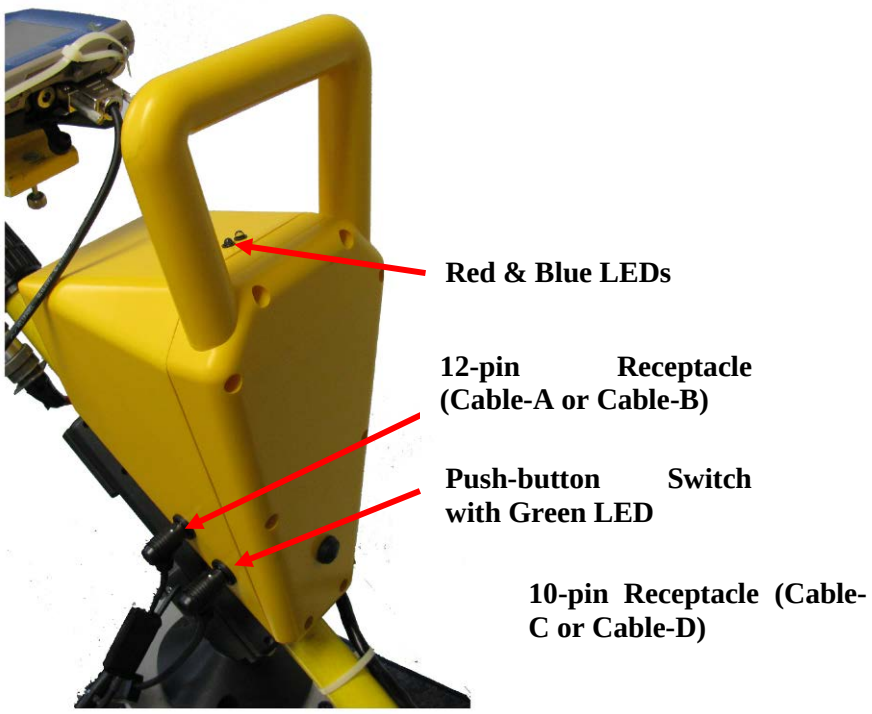

Figure A-2 The SAINT system IMU housing with interface details

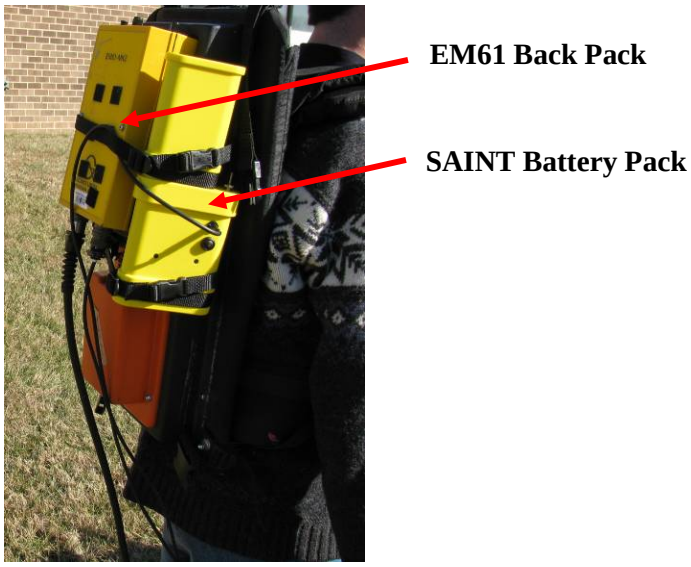

Figure A-3 The SAINT system battery pack strapped to the EM-61 backpack

The new system replaced the all metal tripod used with the prototype. The legs on the new tripod are all non-metallic. The top cone on the tripod where the SAINT sits was broadened to ease the placement of the system on the tripod (see Figure A-4). The cup on the SAINT that sits on the tripod cone has a ruggedized switch to trigger the SAINT timing when it is lifted on/off of the tripod. There is also a notch/key on the cup/cone to re-align the SAINT when it is placed back on the tripod. One leg of the tripod has a footer for the EMI coil to rest on (see Figure A-5). Figure A-6 shows the EM61 coil with a bracket made to fix the coil orientation relative to the rest of the SAINT/EM61 system.

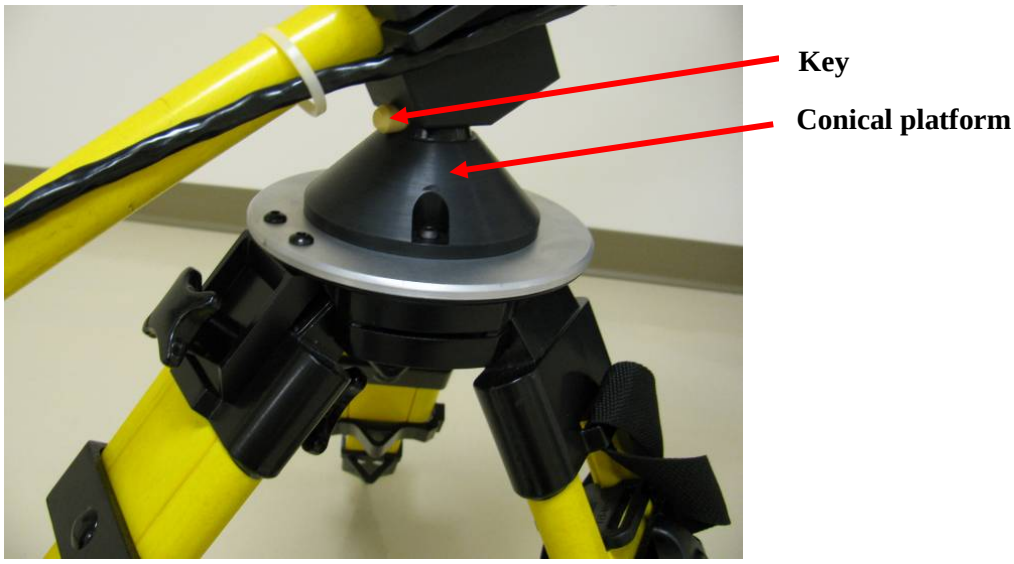

Figure A-4 The SAINT system tripod – base plate details

Figure A-5 The SAINT system tripod – leg details

Figure A-6 The SAINT system coil-locking bracket

Figure A-7 illustrates the general operation of the SAINT. The photos (from left to right) show it being used on a wooden platform designed for general testing. In general, the tripod and SAINT are placed within a meter or two of an anomaly location. The SAINT and EM61 are powered up on the tripod. After sitting idle for 15 seconds of background data, the SAINT beeps once and flashes the blue LED. The user lifts the system and proceeds to sweep the sensor back and forth over the object location. The SAINT beeps and flashes at several intervals during data collection. After 30 seconds of collection it beeps and lights up continuously until replaced on the tripod. After another 15 seconds of being idle, it beeps/flashes once to indicate that it is ready to move again. Examples of actual sweep data are shown below the photos in Figure 7.

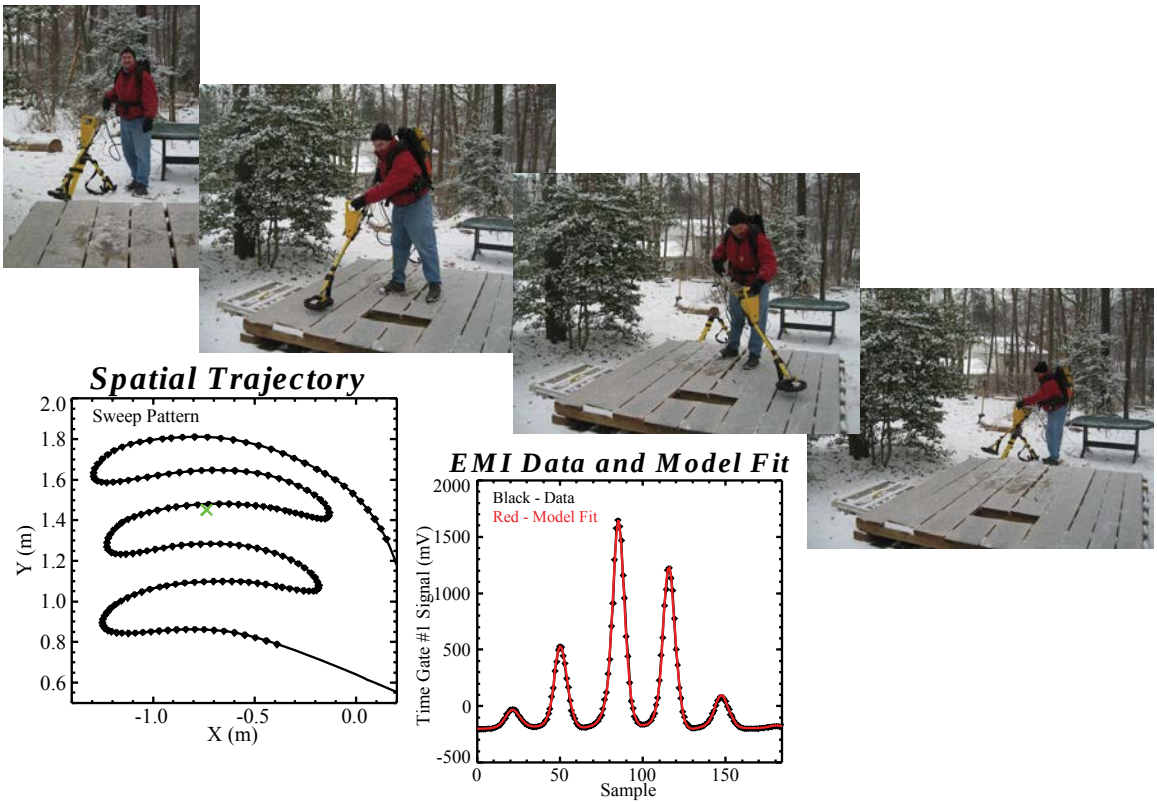

Figure A-7 Standard survey procedures include taking the sensor off of the tripod, waving it above the targets' location, and returning the sensor to the tripod for a zero velocity update (top photographs). The two scatter plots on the bottom show the spatial trajectory of the sensor head (bottom left) and the measured EMI data (bottom right).

After the idle period, more data can be collected over the same object or from nearby objects without moving the tripod. All of the IMU and EMI data would go into the same file on the SAINT. The SBC creates a new file on startup using the nomenclature "FILE_XXX.DAT", where XXX is the current file number. The file number is derived from a configuration file on the SAINT called "SNTCNF.TXT". This text file has the current file number on it. After a file is closed, the current number is incremented. After collecting either a single or multiple runs in a file the system can be either paused or shutdown to close out the current data file. To pause the SAINT, the power button is pressed once briefly. The blue status LED and the green LED on the power button will flash on/off continuously to show that it is paused. The SAINT and tripod can then be moved to a new location. To start at the new location with a new file, the power button is pressed again briefly. To shut the system down, the power button is pressed and held until the SAINT emits a continuous tone. At this time the battery pack's power button should be pressed to shutdown the power to the SAINT.

The SAINT data files are stored by the SBC on a mini-SD card. When started with its USB cable, the SAINT emulates an external USB drive on a PC. The data files

("FILE_XXX.DAT") can be transferred to the PC. To process the IMU data into sensor trajectorys, ENSCO has written an interactive GUI program in Matlab. From the GUI, one selects the data file to process. The data is read in and displayed with the idle periods identified as ZUPT's (Zero-Velocity Updates). An example is shown in Figure A-8. The user selects which periods of motion between ZUPT's to process. The trajectories are calculated and dumped into ASCII files called "FILE_XXX.DAT_imuX.txt". The second X is a number indicating which run within the file has been processed (in the case of multiple runs in a file). The "trigger" times of the EM61 by the Allegro computer and the return times of EM61 data packets are placed in a file called "FILE_XXX.trig.dat". The EM61 data packets are placed in a file called "FILE_XXX.em61.dat". The trigger information and EM61 data files are for the entire file. These text data files are analyzed by SAIC using routines written in an analysis package called IDL. The routines read in the data and automatically match up the EM61 times to the IMU position times. Interactive routines trim out the EM data during a specific run. This data is passed to EMI inversion routines for EM61-HH data. The data and fit results are plotted out in a standard set of diagnostic plots.

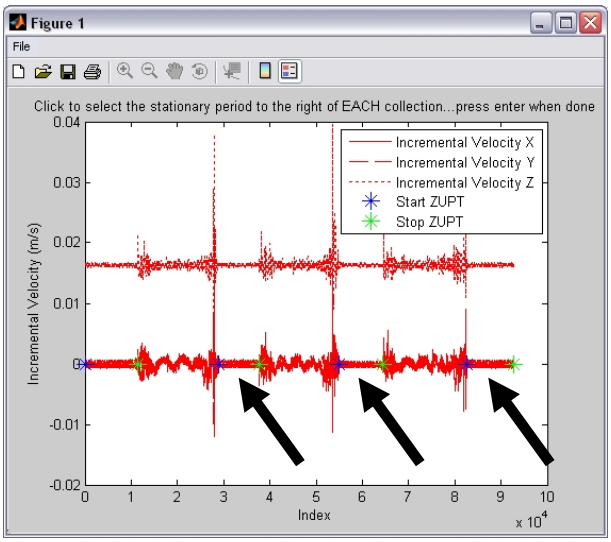

Figure A-8 Select the ZUPT periods (identifiable by a flat line). In this example, there are three stationary periods marked by arrows that should be selected.

Initial Testing

Shake Down of System

The system was built by ENSCO and delivered to SAIC in January of 2009. From January to May of 2009, the system was put through a number of controlled tests. A variety of minor glitches were found and corrected in the hardware/software of the SBC and in the post-processing software. Initially, there were a number of problems with corrupted data. Collecting the IMU packets at 600 Hz, the electronic compass data, the EMI triggers and the EMI data packets was not as easy as ENSCO thought. The status

lights were also not operating properly. It took several iterations between controlled tests and returning the equipment to ENSCO to correct the problems found.

Figure A-9 illustrates one of the simple controlled tests. A set of four poles were set out in a rectangle at a known distance from the tripod. The sensor was lifted from the tripod, moved to the rectangle and would touch each of the four poles. This was done repeatedly in a single data collection. The plot on the left shows the *x,y* trajectory of the sensor for repeated runs. Alternating runs are plotted in red and black. The center of the tripod is at *(0,0)* and the distance to the rectangle's lower left corner is plotted as a dotted arc. Initially, there were problems with the electronic compass data and in post-processing calculations of IMU bias levels during the motionless ZUPT periods. From run to run and to a lesser degree during the run, the heading would drift. The plot on the right shows data collected after these problems were fixed.

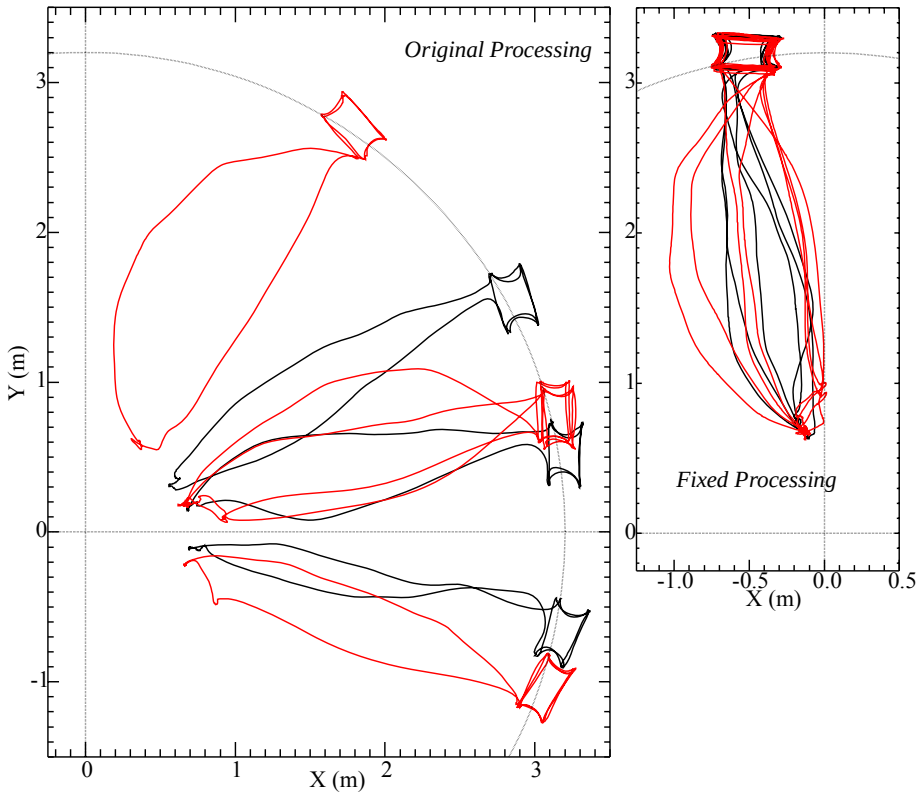

Figure A-9 Controlled test to validate system registration. The test protocal included repeat movements to four poles arranged in a rectangle. The image on the left indicates a problem with the internal compass. The data on the right were acquired after the problem with the compass was resolved.

In order to track the position and orientation of the EMI sensor coil, the SAINT system must know the relative location and orientation of the coil center from the IMU. Roll and pitch angles were checked by collecting controlled data on a flat surface. The system would be lifted from a tripod, placed on the flat surface and then pitched/rolled in

controlled directions. The zero level and sign of the pitch/roll angles could be checked in this fashion. To check the yaw angle and *(x,y,z)* displacement settings, a chalk circle was drawn on the flat surface. Distances and angles were carefully measured from the tripod and the starting location of the sensor coil to the circle. A set of fixed angles were marked (30, 60, 90, 120, 150 degrees). The coil was lifted from the tripod, moved straight forward to the circle and then swept along the circle stopping at the marked angles. Figure A-10 plots these trajectories with the original (left plot) and corrected *(x,y,z)* displacements (right plot). The black solid curve is the coil center trajectory. The red dashed curve is the circle that the coil center was meant to track. The inner dotted circle is the actual chalk circle that the operator traced with the back of the EMI coil, because the operator can not actually see the coil center. The dotted rays are the fixed angles that the sensor paused at.

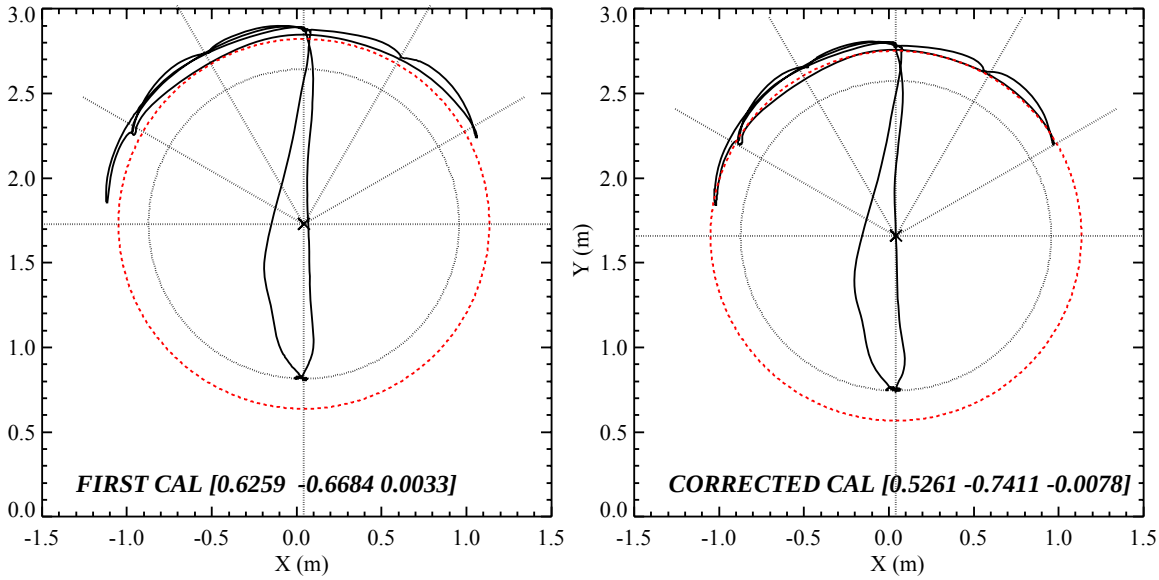

Figure A-10 Controlled test conducted on a flat surface to check the pitch, roll, and yaw angels as well as the displacement settings. See text above for details.

The SBC times everything by the current IMU data packet. The EM61-HH is triggered by the Geonics software running on a handheld Allegro computer. The SBC monitors and time stamps the serial trigger sent by the Allegro as well as the data packet sent back to the Allegro from the EM61-HH electronics. To check for accurate time stamping by the SBC, the EM61-HH data on the Allegro computer was compared to the same packets captured on the SBC. After initial fixes to correct missed and corrupted EM61-HH data, the timing of the two data sets matched reasonably well. The top plot in Figure A-11 matches the data as a function of sample number between the packets recorded by the SBC (in black) and the packets recorded by the Allegro (in red). The data shows the system being swept over an object three separate times. The two plots below this graph the time steps between data packets as recorded by the two systems. The data rate was roughly 15 samples per second (0.067 s). The Allegro software (third plot, in red) plots

time steps to an accuracy of 0.01 s. There are occasional long time steps on the order of 0.14 s. The SBC (second plot, in black) should be able to time stamp the data to within several IMU time counts at $1/600^{th}$ of a second (0.0017 s). The observed jitter in time steps is much larger. It does match the Allegro on most of the larger time steps. It would appear that every now and then the Allegro misses sending a trigger. However, the SBC also has several other large steps not recorded by the Allegro where triggers are being either missed or incorrectly time stamped. After further work on the SBC software, better results were achieved. The last two plots show fixed SBC (black) and Allegro (red) time steps. Better results were achieved on the Allegro timing by using newer software for Geonics EM61 systems produced by a company named Geomar. The Geomar software could time tag the data to within 0.001 s with jitter on the order of several samples. There were fewer large time steps in the data as well. The improved SBC software showed jitter on the order of several IMU data packets, 0.0017 s. It reasonably matches any larger time steps on the Allegro and had few if any glitches not matched by the Allegro. Overall, the IMU and EMI data streams are matched to within 5-10 milliseconds.

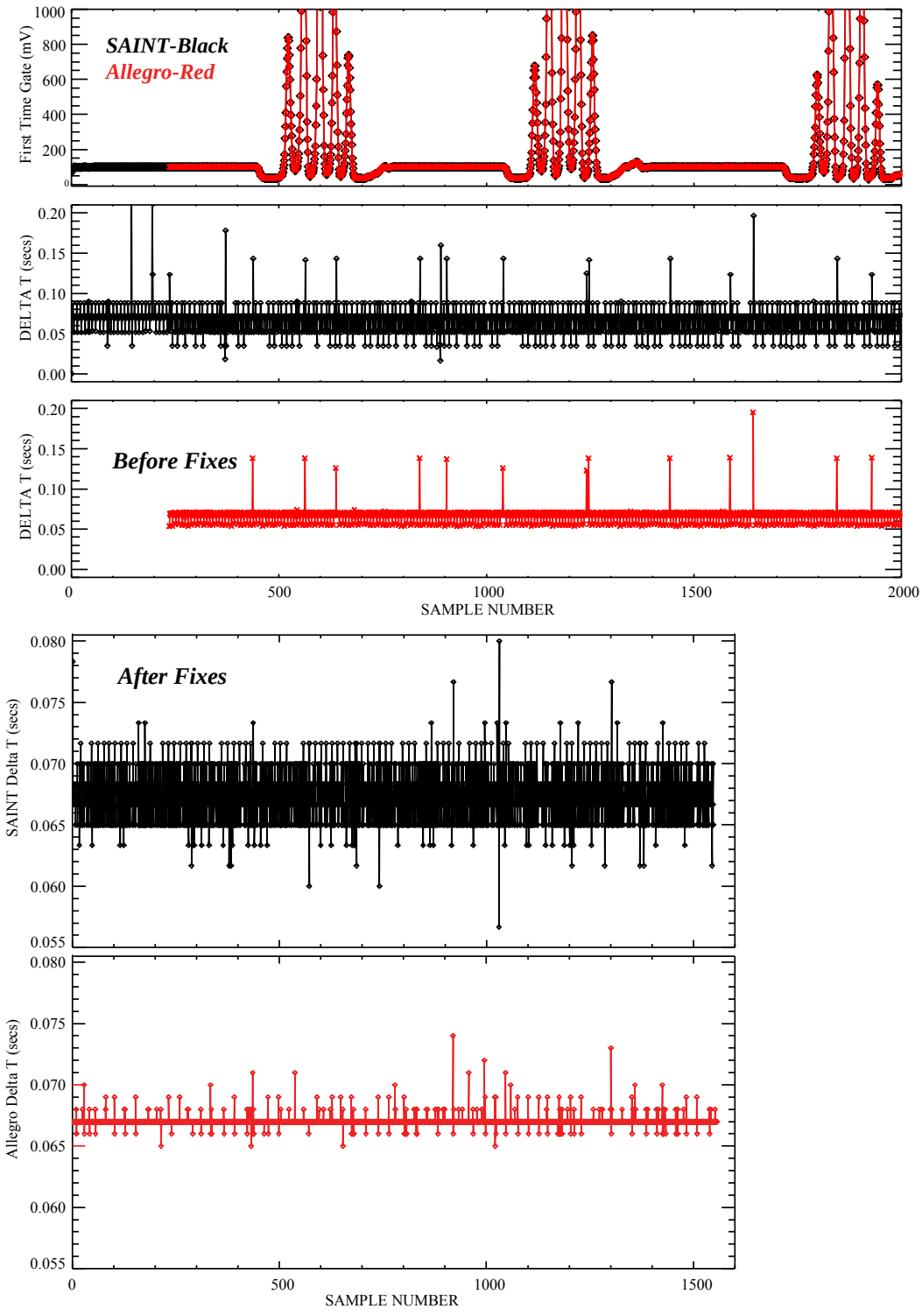

Figure A-11 Raw time series as timed by a SBC and logged by the SAINT. See text above for additional information.

Sweep Pattern Testing

Concurrent with the shake down, testing was done to determine if different sensor sweep patterns would collect better data for EMI inversion. For the operator, the easiest sweep pattern is to just move the sensor back and forth, side-to-side. Within the constraint of 30 seconds for data collection, it is possible to obtain 5-6 slices of data over a buried object. Because the EM61-HH is a bistatic sensor (transmit and receive coil not co-located), a buried object would be better covered by the sensor if it passes over the object in several directions.

Figure A-12 illustrates a simple back and forth sweep in the upper left plot. A multiple direction, "X" pattern sweep is shown in the upper right. Other sweep patterns were tested as well, but most were not easily performed by the operator in the time allowed. Note that in the simple sweep pattern, the heading of the sensor is kept relatively constant (along the y-direction). With the "X" pattern, there are 3 similarly oriented passes, but the two "X" passes are oriented at ±45 degrees to the y-direction. The data collected by these sweeps are shown as a function of time in the plots below. The symbols in the upper plots are the *x*,*y* locations of the measured EMI data plotted with the same symbols in the lower plots. The red curves in the lower plots are the best model fits to the data from the EMI inversion.

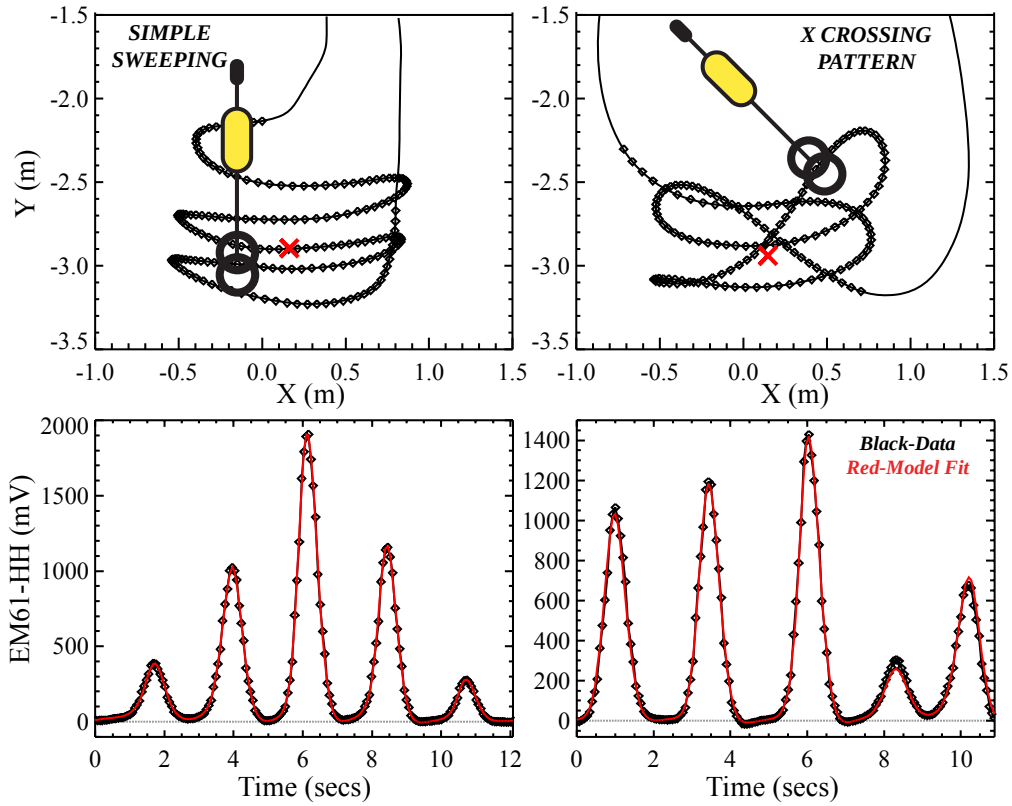

Figure A-12 Example data set showing the spatial sweep pattern (top) and rastorized EM61 HH data (bottom). The two data streams are merged to create a spatially registered data file.

SAINT data was collected multiple times over the same object with these two sweep patterns. The data was inverted using standard EMI dipole modeled based algorithms. The model parameters of location, depth, and magnetic polarizations ("betas") for each time gate were obtained. The expectation was that a more consistent set of inverted parameters would be obtained with the "X" pattern sweep; since, this pattern collected a more diverse set of EMI data from the object. The exact opposite of this was observed. Figure A-13 plots an example of this result. These plotted fit results are from eight simple sweeps and eight "X"'ing sweeps measured over a four inch steel sphere roughly 0.28 m below the test stand. The black plotted symbols are the inversion results from a simple sweep and the red symbols are for the "X" one. The left plot shows the fitted primary beta response versus the fitted depth. The right figure shows the secondary versus primary beta responses; for a sphere, these should be equal. The observed spread is significantly larger for the "X" pattern sweeps.

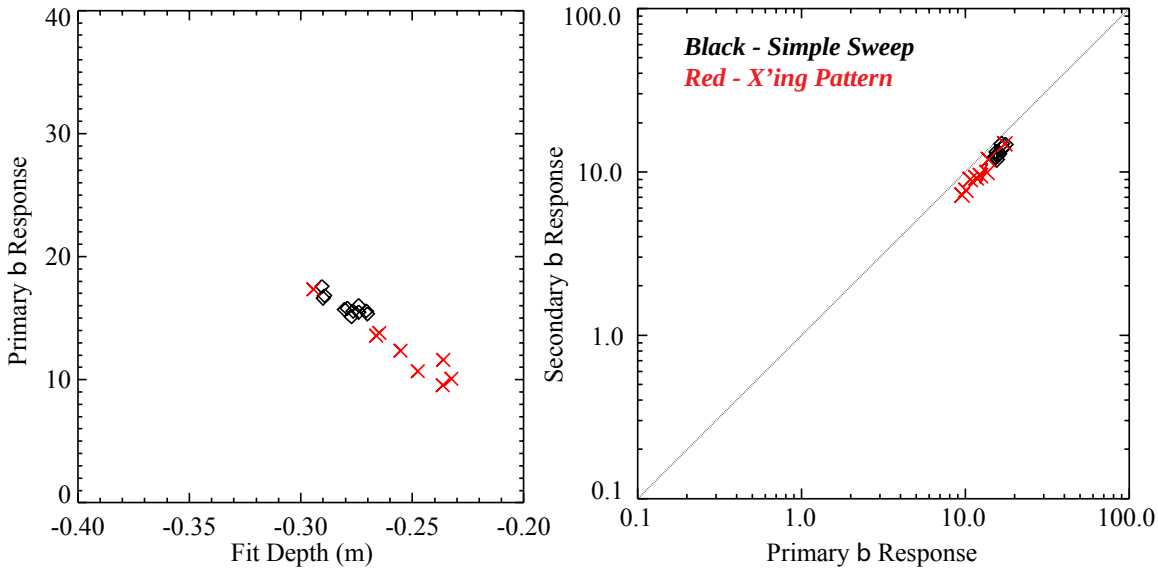

Figure A-13 Comparison of polarizations derived for 8 repeated measurements of a common object for simple sweeps and X sweep patterns.

Sweep Pattern Simulation

Without a way to determine the true trajectory of the SAINT system, it is difficult to diagnose the unexpected results. Past work has shown that EMI inversion is very sensitive to position errors [REF 6], but little has been done to consider different types of position error. One suspicion was that the inherent nature of IMU based positioning was having an effect. Because the IMU measurements are integrated to determine the sensor's trajectory, the position errors tend to be a systematic drift from the true sensor position. GPS, RF ranging, and laser ranging are more likely to produce random errors about the true sensor trajectory. To test this idea, measured sensor trajectories were used in a simulation to compare the effect of the two different position errors on EMI inversion results.

A set of measured simple sweeps and "X" sweeps were used as true trajectories in a simulation. For each run of the simulation, one of these sweeps was randomly chosen. A random *x,y* object location was generated near the center of the sweeps (within 0.05 m). The forward model for the EMI sensor was run for this trajectory and location with a fixed depth of 0.3 m and a set of equal (sphere) beta polarizations of 14.0 m^3. Position noise would be added to the "true" trajectory and then the data would be inverted.

Three types of noise were added to the trajectories: no noise, random noise, and a systematic drift that varied over time. The random noise was generated with a random number generator with a standard deviation of 0.005 m. These random shifts were added in the *x, y,* and *z* directions. Different magnitudes of random error were tested, but the final level used was based on past work that indicates SAINT position errors of less than one centimeter overall [REF 4]. The top plot in Figure A-14 shows an example sweep without (as a black curve) and with random position errors (red symbols). The drift errors were generated by taking 5 points along the trajectory evenly spaced over time. A set of random displacements were generated for each of these five locations. The magnitudes of these displacements were fixed to be less than 0.01 m. From these five shifts, a spline fit was done for *dx, dy,* and *dz* as a function of time. These splined shifts would be added to the true *x, y, z* trajectory. The lower plot in Figure 1 shows an example of this drifted trajectory.

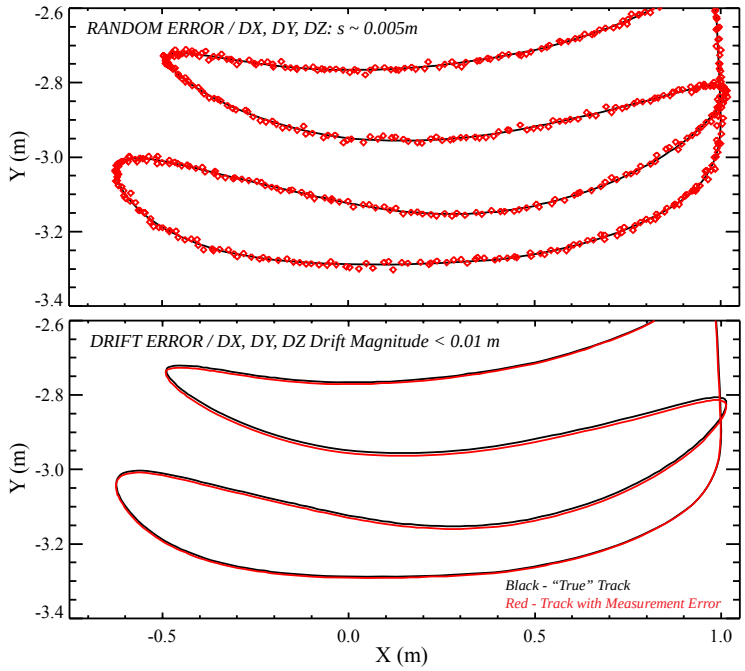

Figure A-14 Graphical display of a sensor trajectory without positional noise (black), with random deviations (red top), and with drifting (red bottom).

For each type of noise, the simulation was run several hundred times. For each run the inversion was carried out over a range of fixed depths and the chi-square value and RMS

fit error recorded. These "Goodness-of-Fit" curves as a function of depth are a good indication of how well the fit algorithm with the data it is given will converge to the correct result. Steeper curves converge well; curves with multiple minima can converge to the wrong answer. Examples of these curves are shown in Figure A-15. Each plot shows the curves for ten different runs of the simulation. The left plots are based on simple sweeps and the right plots are from "X" sweeps. The top set are from simulation runs with no position errors. With no errors, the both types of sweeps has the correct global minimum at a depth of -0.3 m, but the "X" sweeps are steeper, and the simple sweeps show signs of secondary minimums. The middle sets of plots are with random position errors. The curves are broader and the global minimum is not always exactly at -0.3 m. Again, the simple sweeps are not as good and show distinct secondary minima. The bottom set of plots are with drift position errors. In this case, the simple sweeps are the better set of curves; the global minima are close to -0.3 and the secondary minima are no worse than before. The "X" sweeps show global minima over a larger range as well as some secondary minima. The fit error at some of the minima has also become significantly larger.

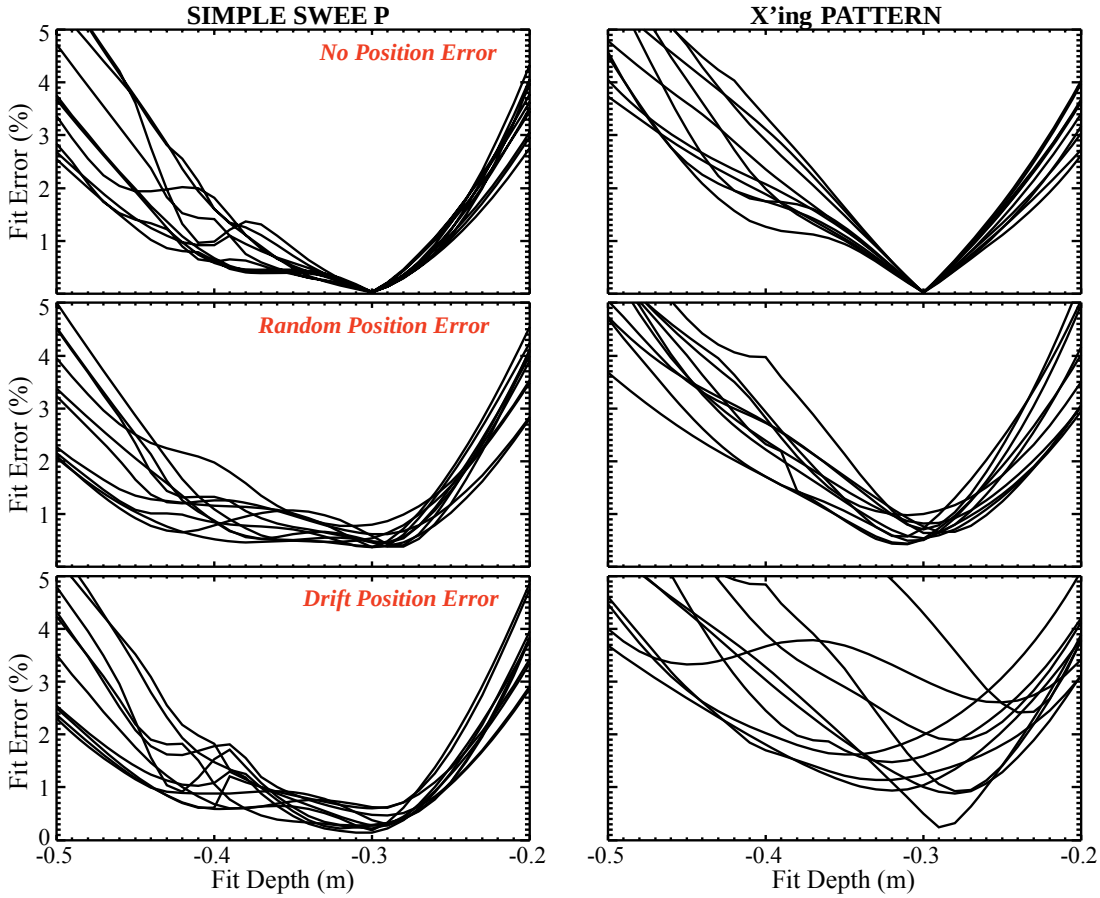

Figure A-15 Goodness of fit curves for two surveys and three distinct noise scenarios. There are ten runs (curves) for each case – see text above for additional details.

Figure A-16 plots the best fit parameters for these different position error cases. The symbols plot the fitted depth and fitted primary beta polarization for one hundred runs of the simulation. Again, the left plots are for simple sweeps and the right plots are "X" sweeps. The top plots are with random position errors and the bottom for drift errors. With random errors, the "X" pattern produces a smaller spread in the fit parameters, but for drift errors a sweep pattern gives the better result. While these spread patterns are not exactly equivalent to the measured results in Figure 2 (of previous section), they do seem to indicate that drift errors are the source of the SAINT system EMI inversion spread and that a simple sweep pattern is more robust in the face of these errors. In general, any EMI data collection and inversion will be more sensitive to systematic position errors than random ones.

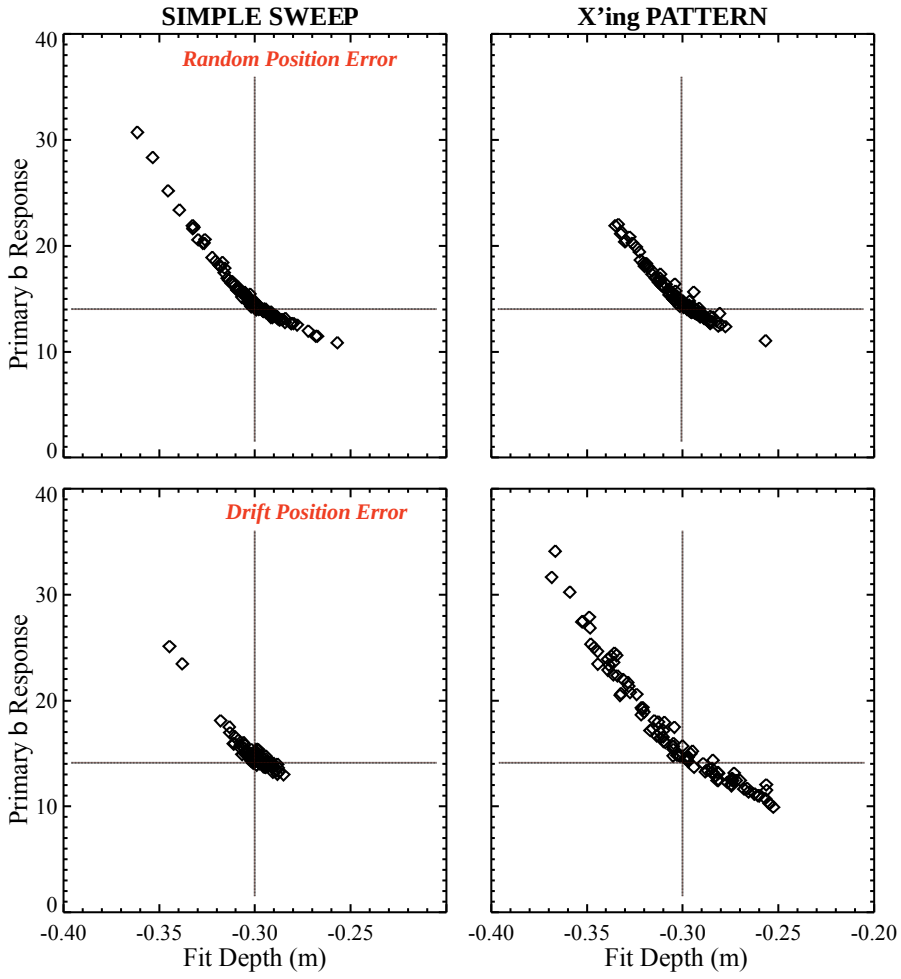

Figure A-16 Fitted parameters for two sweep options and two types of position errors.

Test Stand Measurements of APG Targets

To prepare for a demonstration of the SAINT at the Aberdeen Proving Ground (APG) Standardized UXO Technology Test Site, a set of the possible UXO target items was obtained. Because the SAINT system is designed for local interrogation of items already detected, it was decided to take the SAINT to the Blind Grid scenario only. There are six possible UXO items buried there: 25mm, 37mm, 60mm mortar, 81mm mortar, 105mm, and 105mm HEAT. These are shown in Figure A-17. These items were placed under a wooden test stand and measured repeatedly at different depths and orientations.

Figure A-17 Photograph of the six munitions at APG

A simple sweep pattern was used and repeated four times to check for variability in the EMI inversion results. It was found that the variability could be minimized by keeping the collection time to a minimum and by limiting the amount of change in the sensor heading. This resulted in a very fixed data collection routine as illustrated in Figure A-18. The tripod would be placed about 1 m to the right and 1.5 m away from the "flagged" location. The SAINT system would be lifted from the tripod and moved straight forward. It would then be moved left/right back and forth in a series of six passes without significantly changing the sensor heading. On arbitrary surfaces such as the test stand and grassy fields, it was found to be useful to place a marked board on the ground. The board had marks every 0.12m. This helped guide the operator and insured uniform coverage over the flagged spot. Each collection was on the order of 15-20 seconds. With 15 sections of stationary data before and after each collection, total time for four data collections over an object was about 2-3 minutes.

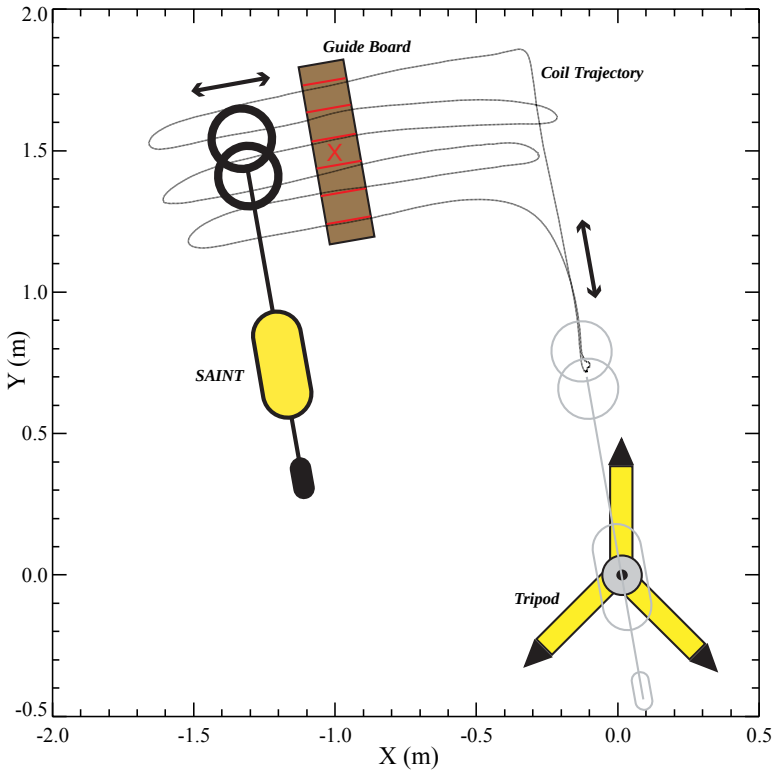

Figure A-18 Schematic illustrating the data collection concept of operations.

Figure A-19 shows the result of multiple sets of measurements over a 60mm mortar at a variety of depths and orientations. The top plot shows the 3 beta polarizations (1st time gate) inverted from the data as a function of data run. The black symbols are the primary beta and the red/green symbols are the secondaries. The dashed lines indicate the average value. The bottom plot shows the fitted betas on a log-log scale. The symbols are plotted at the primary beta value and the average of the secondary. The line through each symbol represents the range of the two secondaries. The average values are shown as dotted lines. Overall, there is reasonable clustering, but outliers remain.

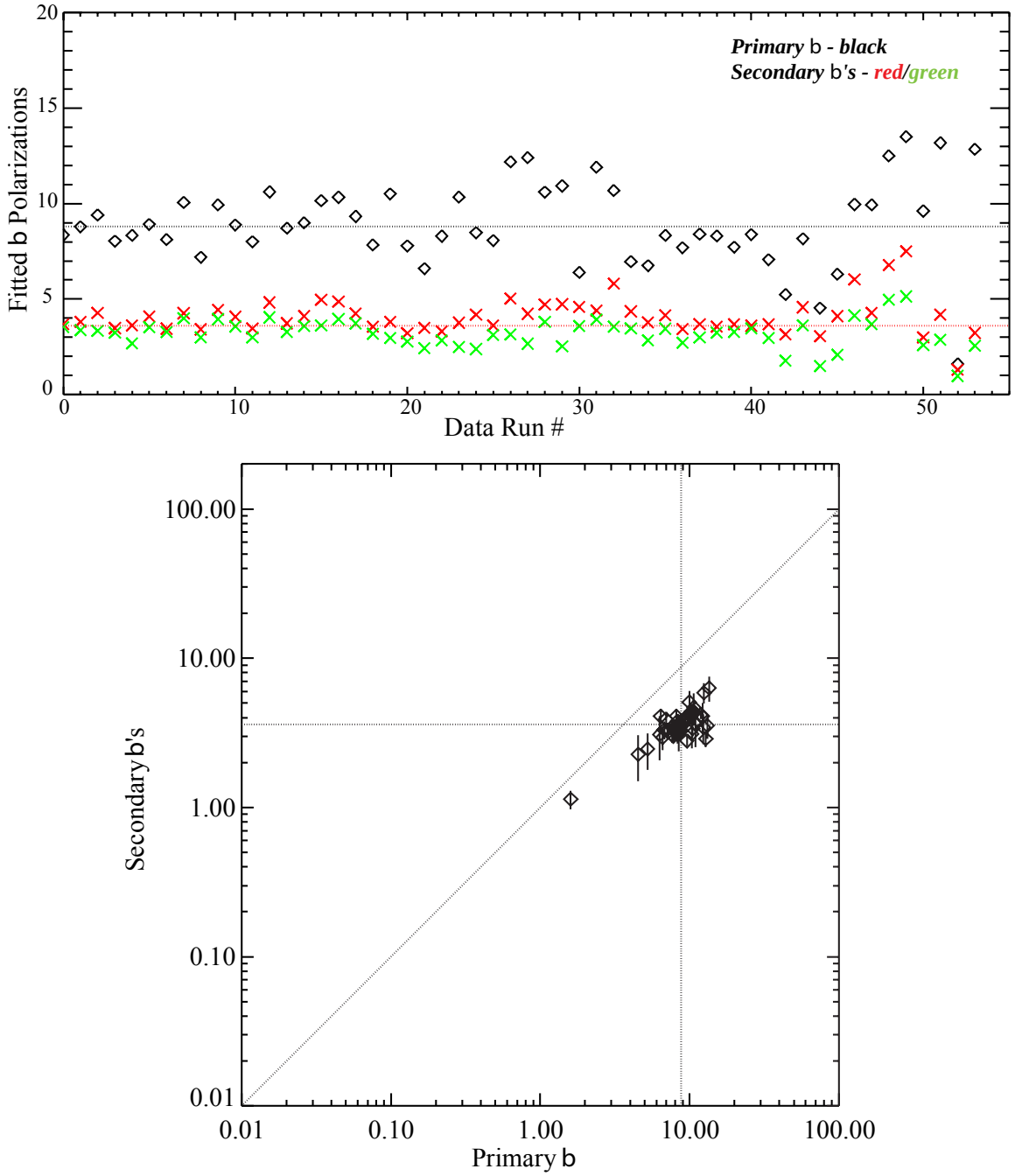

Figure A-19 Fitted parameters for multiple 60mm mortars at a variety of depths and orientations.

Figure A-20 shows on log-log plots the fitted betas from measurements over an 81mm mortar. The left plots show results for the 1st time gate and the right plots are for the 4th time gate. The top two plots are for moderately tilted and horizontal 81mm's. Similar to the 60mm plot above, there are some outliers. The bottom plots are for 81mm's oriented nearly vertical, nose down. In this orientation, the aluminum tail fin of the mortar dominated the signal and resulted in very different values for the polarizations. Instead of

the ferrous, cylindrical solution found for most UXO ($\beta_x > \beta_y = \beta_z$), it gave a ferrous plate-like solution ($\beta_x = \beta_y > \beta_z$). The "logarithmic" circles in Figure 4 represent the final set of beta polarizations used to identify the buried UXO at APG. Each circle is centered on the average value obtained for the item from test stand and APG Calibration Grid measurements. The "log" circle diameter is of arbitrary size, but does a reasonable job in capturing most of the betas for a given object. The circles are identified in the lower, right plot. The dashed circle represents the results from aluminum tail fins. These "fin" results were obtained for both the 81mm mortars and the 105mm HEAT. There was some scatter in results for the larger ordnance between nose up and nose down orientations, but the UXO library set plotted was adequate to capture most of this data. It was found that only a single set was needed for the 105mm (any orientation) and 105mm HEAT (horizontal). This is probably an indication that the early time gates of the EM61-HH are not very good for distinguishing between large ordnance.

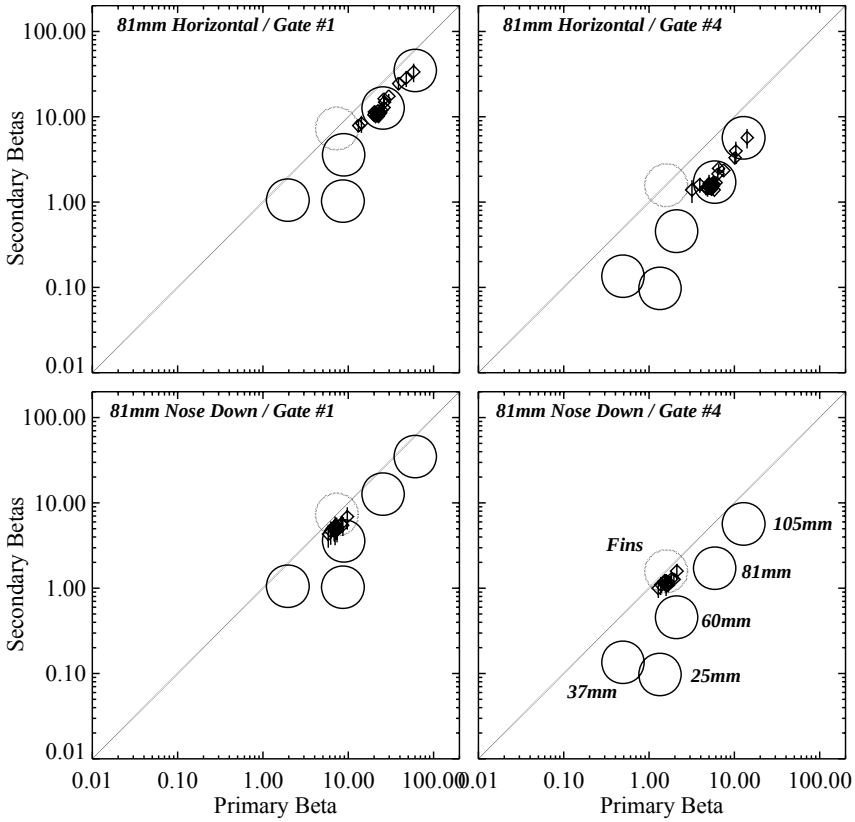

Figure A-20 Fitted parameters for an81mm mortar in different orientations

Based on these test stand results, the final strategy for the SAINT at the APG demonstration was to take four sets of data over each item. A set of diagnostic plots was developed to check on both the data and fit quality. Samples of these plots are shown in

Appendix A. The data was fit unconstrained in beta polarization values for the four time gates and then re-fit with the library of expected UXO values for all 4 gates. The best library fit was kept. To identify UXO from clutter, a library ratio test was used. The ratio of the library to unconstrained fit error was calculated. If the ratio approached 1.0, both fits were equally good and the item was likely the identified item. If the ratio was small (by observation < 0.98), the item could not be fit well by the UXO library and was most likely clutter.

Test measurements were also taken before the demonstration with items placed in a hole in the ground. Measurements at the test site found a large gradient in the EMI signal from the ground. The 1st time gate of the EM61-HH varied over 100 mV within 0.10 m from the ground surface. It was found that the SAINT system could be used to make a quick vertical profile of the sensor ground response. It could track the sensor coil height as it was raised and lowered from the surface over an area with no buried objects. Figure A-21 plots this ground response data at the test site (black curve) and at the Aberdeen Proving site (red curve). If there is a large gradient as the sensor is swept about over the ground, small changes in height above ground could produce noise in the signal. Because of the test site gradient, the sensor had to be swept about at a height of 0.15 to 0.2 m to minimize this noise. At APG, there was no measurable signal from the ground. The sensor was swept about as close to the surface as was possible.

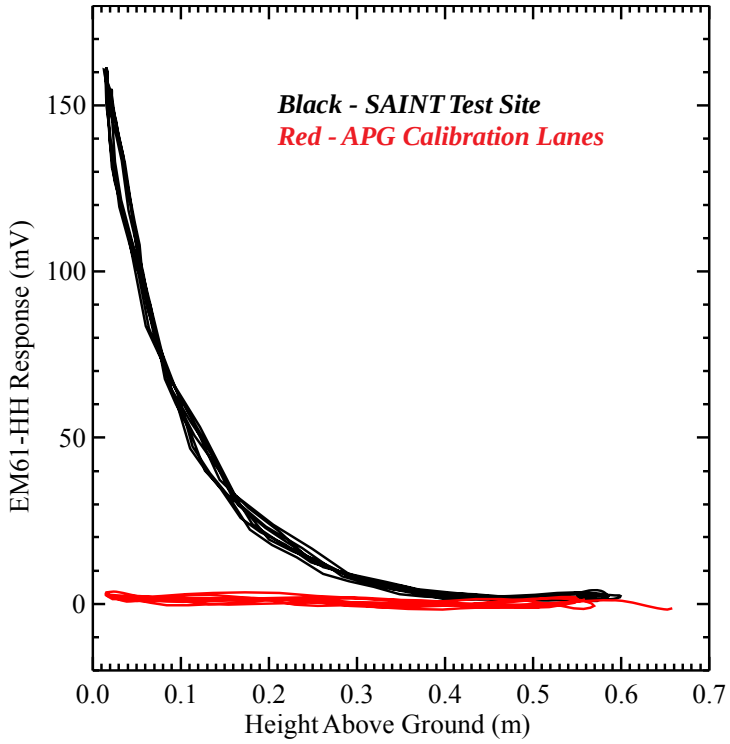

Figure A-21 Comparison of sensor response as a function of height at two sitess

APPENDIX B – DATA DIAGNOSTIC PLOTS FOR EM61 HH & SAINT POSITIONING

May21st2009_37mmNSHorizA.Fits.

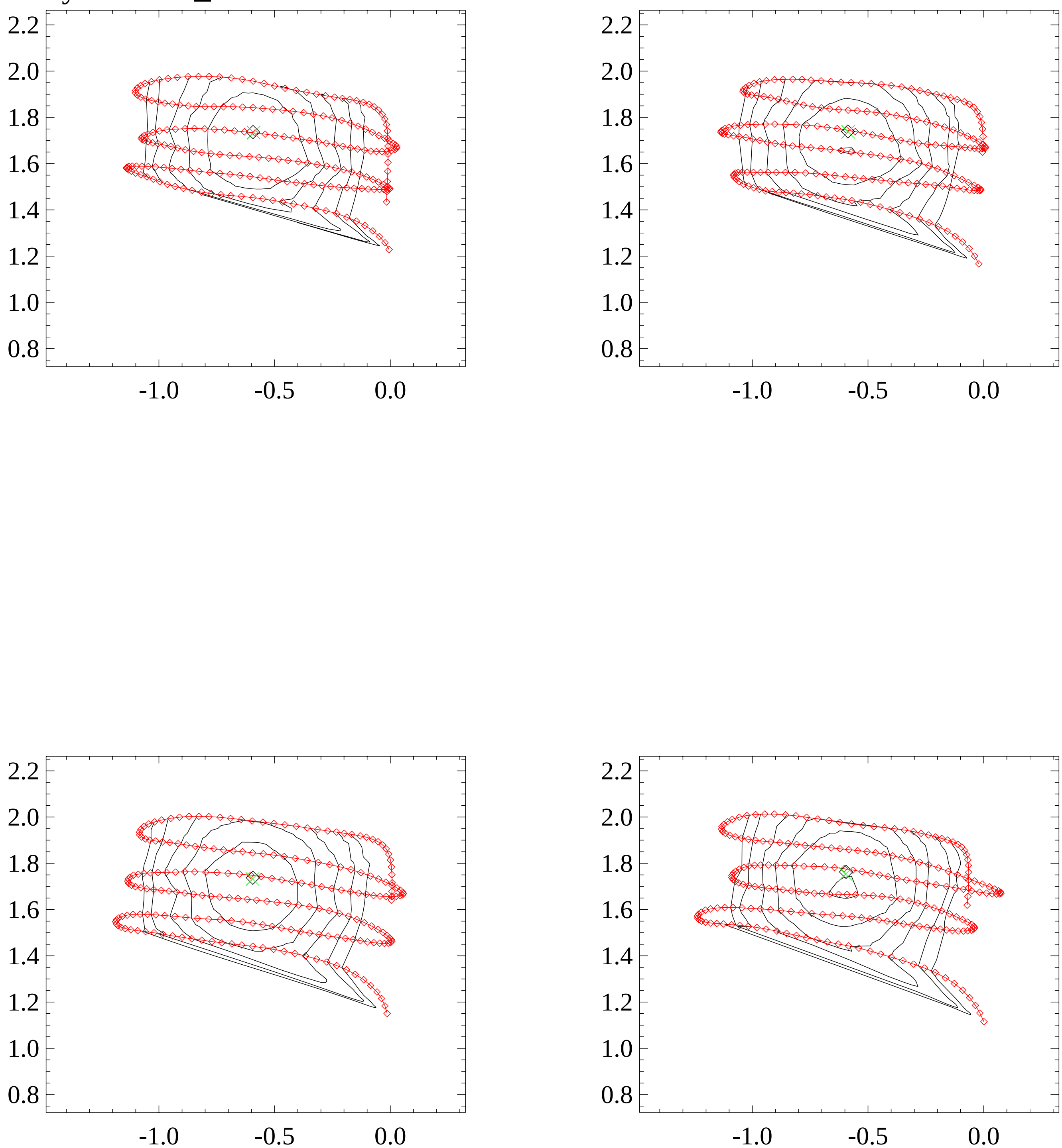

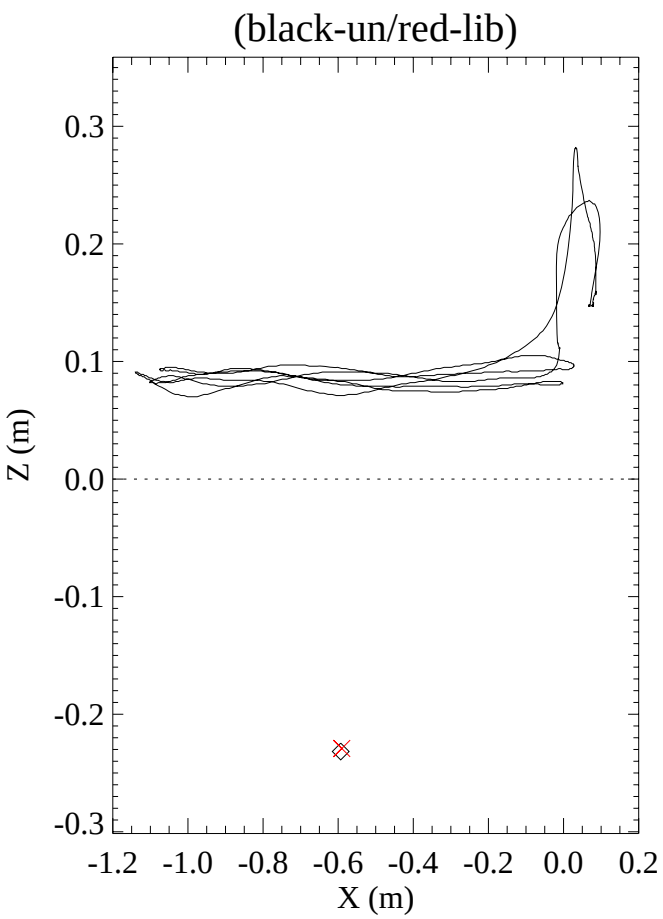
(black-un/red-lib)
0.3
0.2
0.1
0.0
-0.1
-0.2
-0.3
Z (m)
-1.2 -1.0 -0.8 -0.6 -0.4 -0.2 0.0 0.2
X (m)

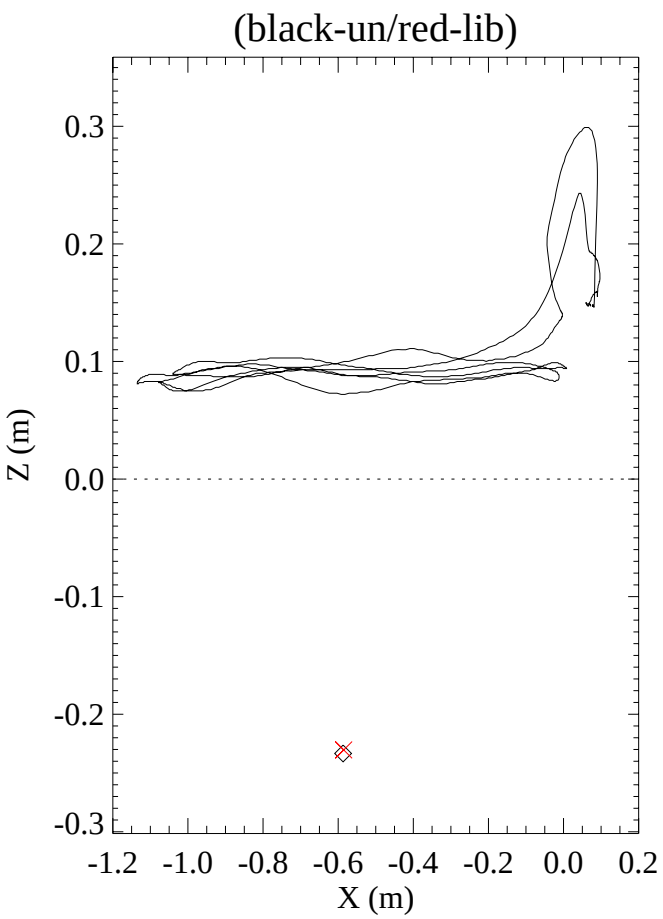
(black-un/red-lib)
0.3
0.2
0.1
0.0
-0.1
-0.2
-0.3
Z (m)
-1.2 -1.0 -0.8 -0.6 -0.4 -0.2 0.0 0.2
X (m)

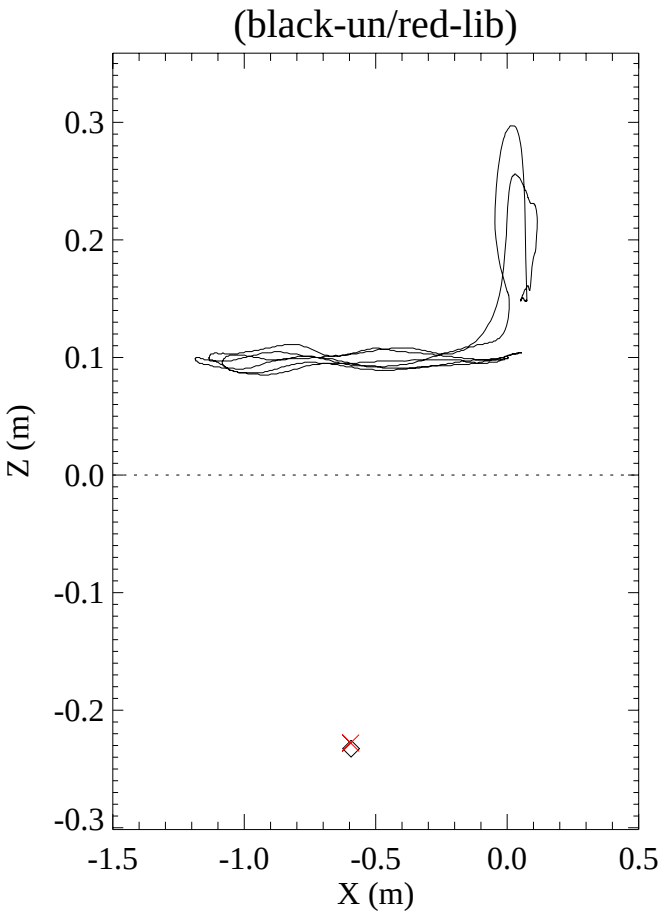
(black-un/red-lib)
0.3
0.2
0.1
0.0
-0.1
-0.2
-0.3
Z (m)
-1.5 -1.0 -0.5 0.0 0.5
X (m)

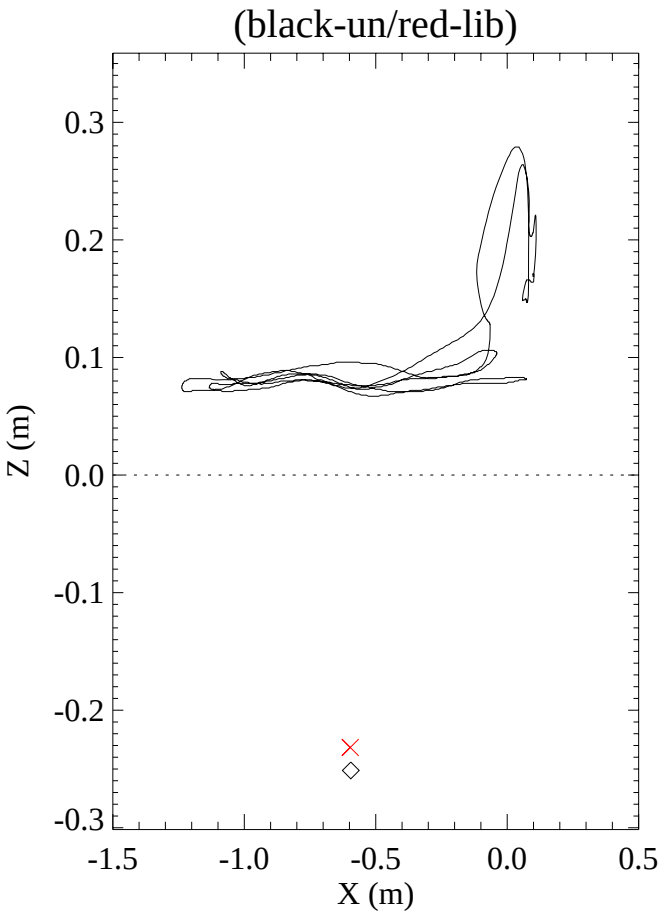
(black-un/red-lib)
0.3
0.2
0.1
0.0
-0.1
-0.2
-0.3
Z (m)
-1.5 -1.0 -0.5 0.0 0.5
X (m)

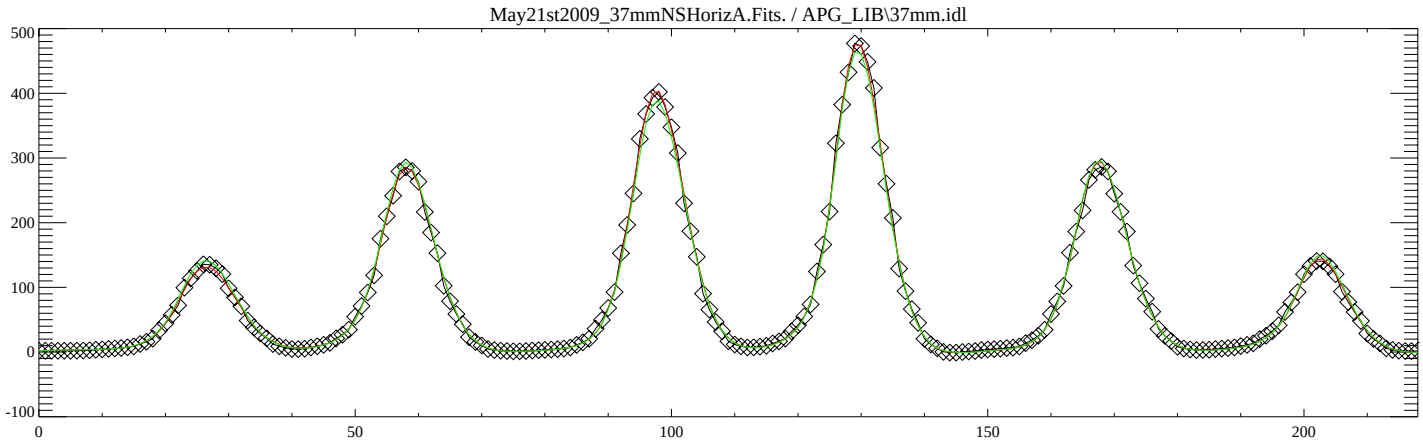
May21st2009_37mmNSHorizA.Fits. / APG_LIB\37mm.idl
500
400
300
200
100
0
-100
0
50
100
150
200

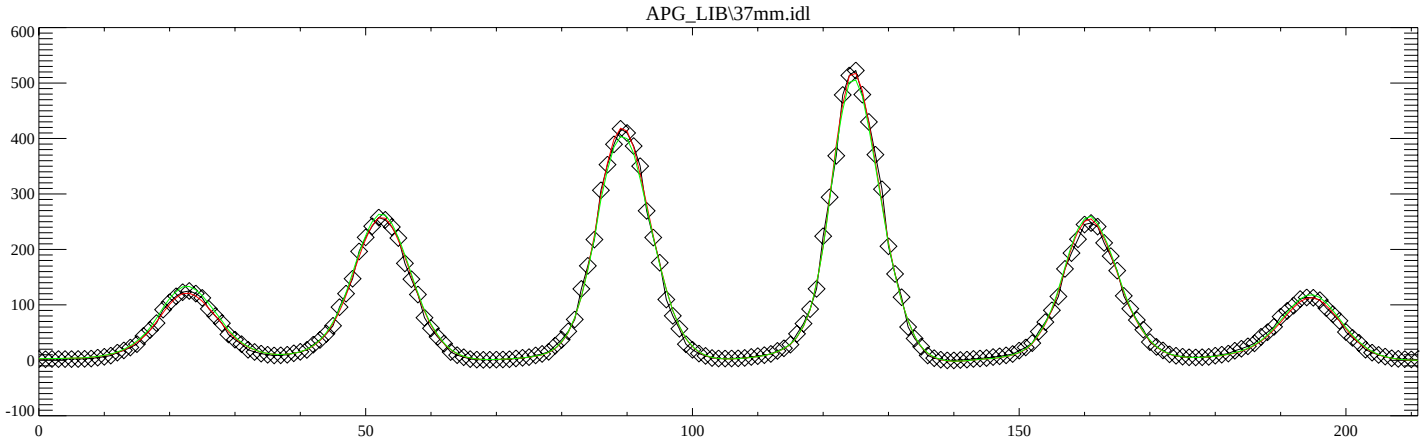
APG_LIB\37mm.idl
600
500
400
300
200
100
0
-100
0
50
100
150
200

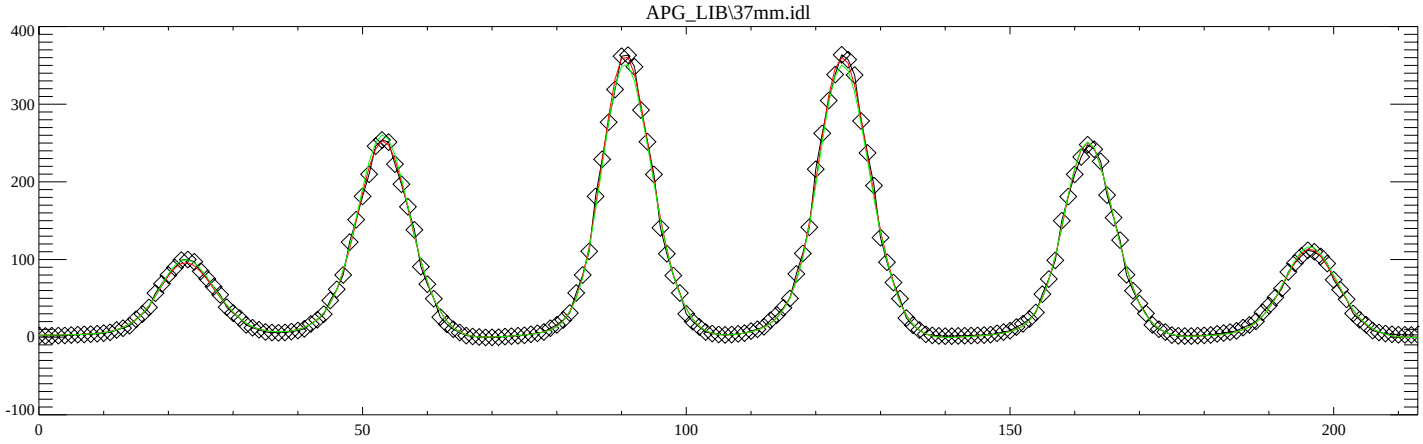
APG_LIB\37mm.idl
400
300
200
100
0
-100
0
50
100
150
200

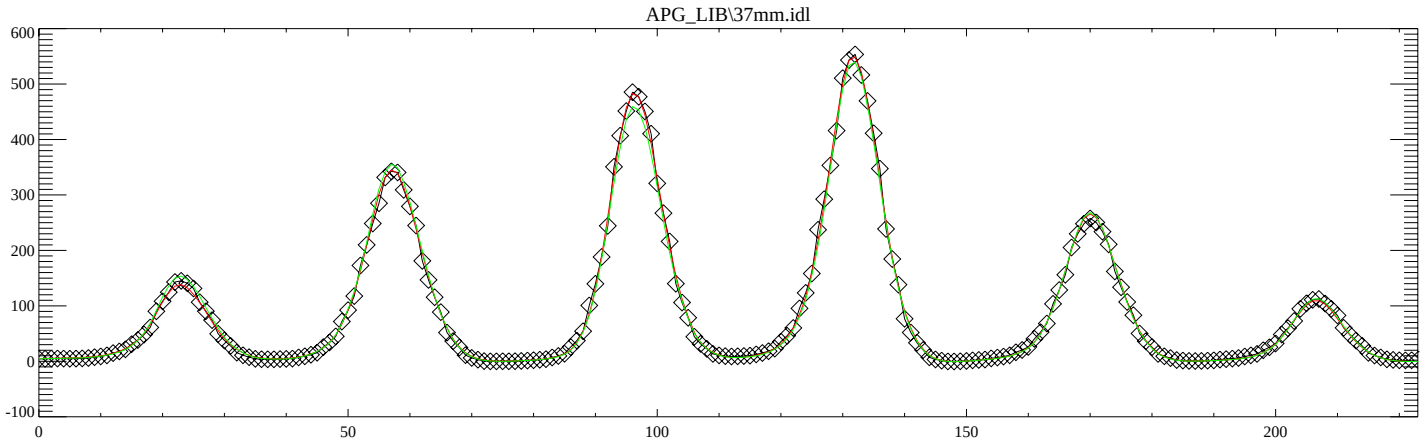
APG_LIB\37mm.idl
600
500
400
300
200
100
0
-100
0
50
100
150
200

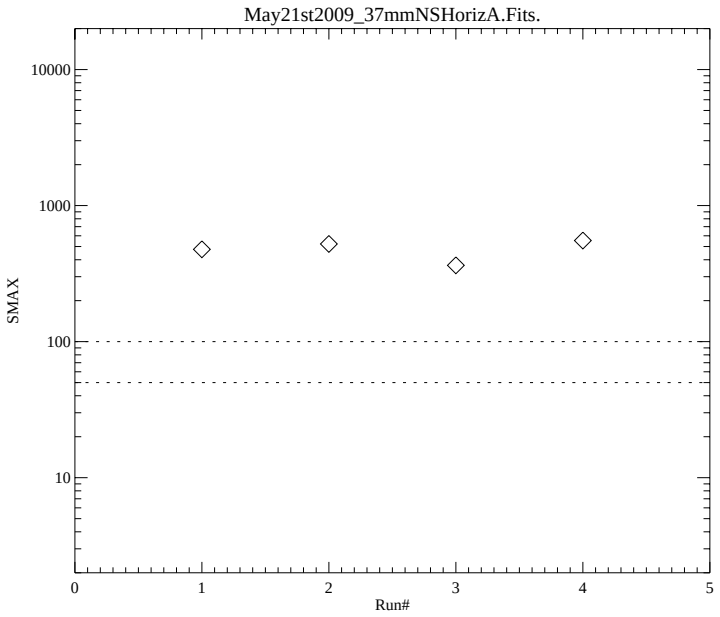
May21st2009_37mmNSHorizA.Fits.
SMAX
Run#

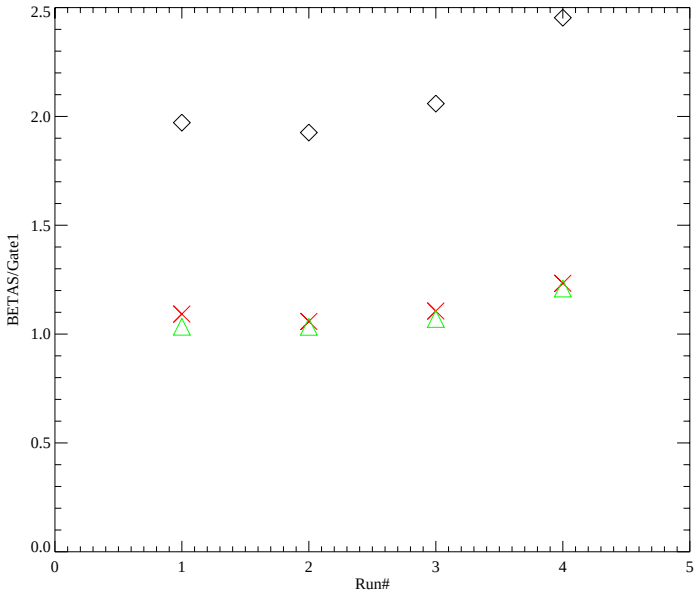
BETAS/Gate1
Run#

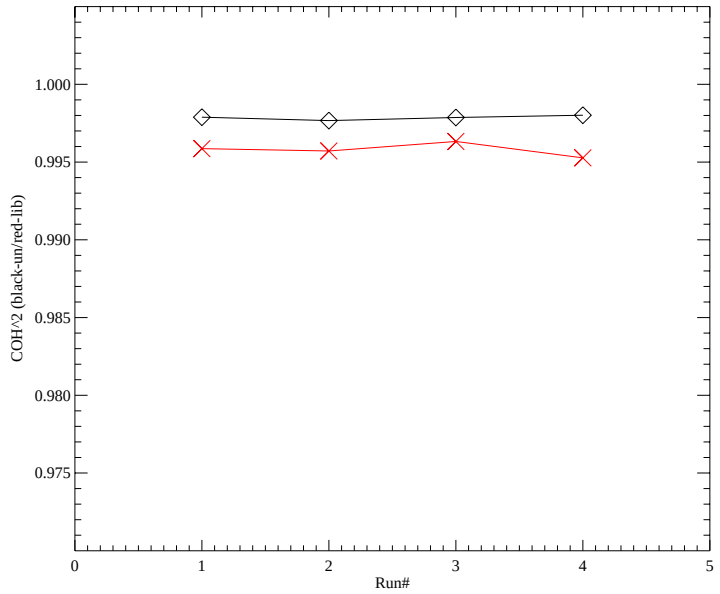
COH^2 (black-un/red-lib)
Run#

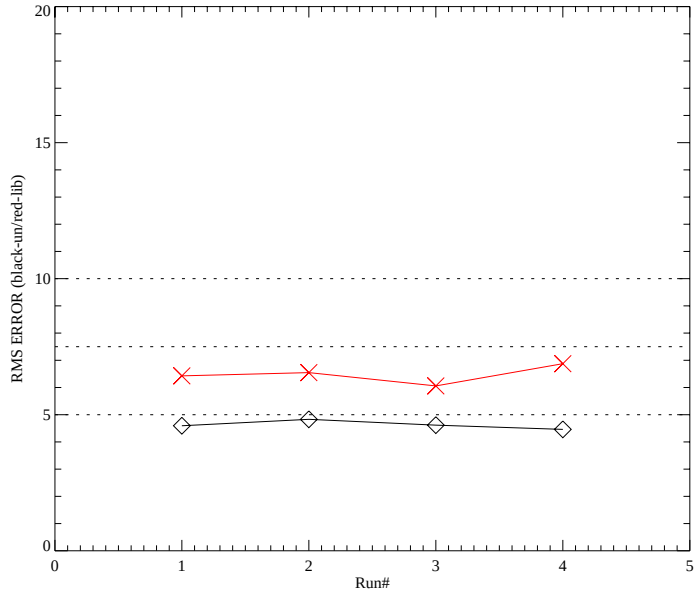
RMS ERROR (black-un/red-lib)
Run#

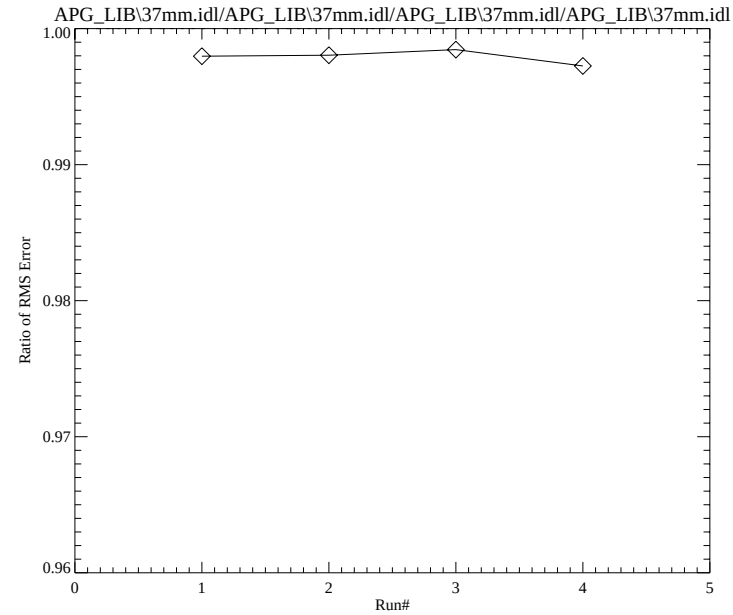
APG_LIB\37mm.idl/APG_LIB\37mm.idl/APG_LIB\37mm.idl/APG_LIB\37mm.idl
Ratio of RMS Error
Run#

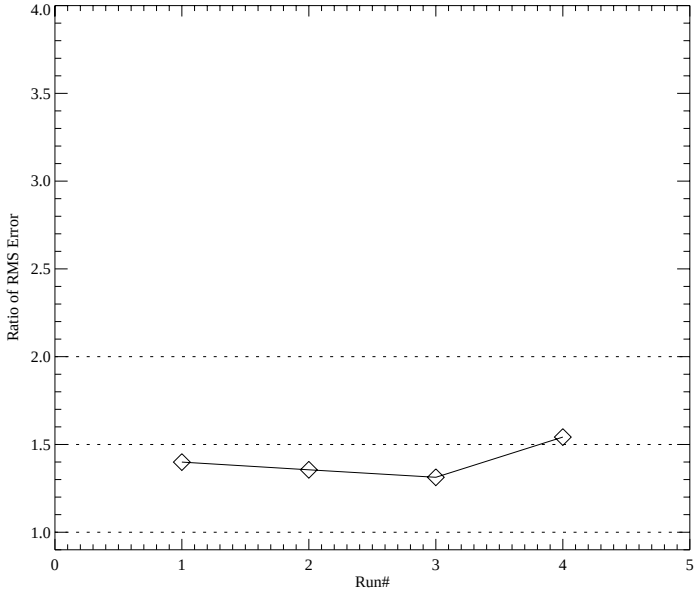
Ratio of RMS Error
Run#

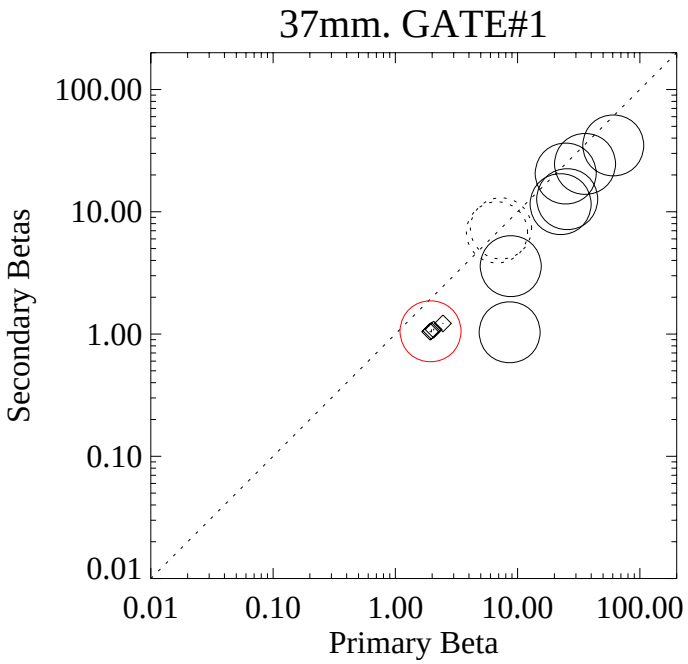
37mm. GATE#1
Secondary Betas
Primary Beta
100.00
10.00
1.00
0.10
0.01
0.01
0.10
1.00
10.00
100.00

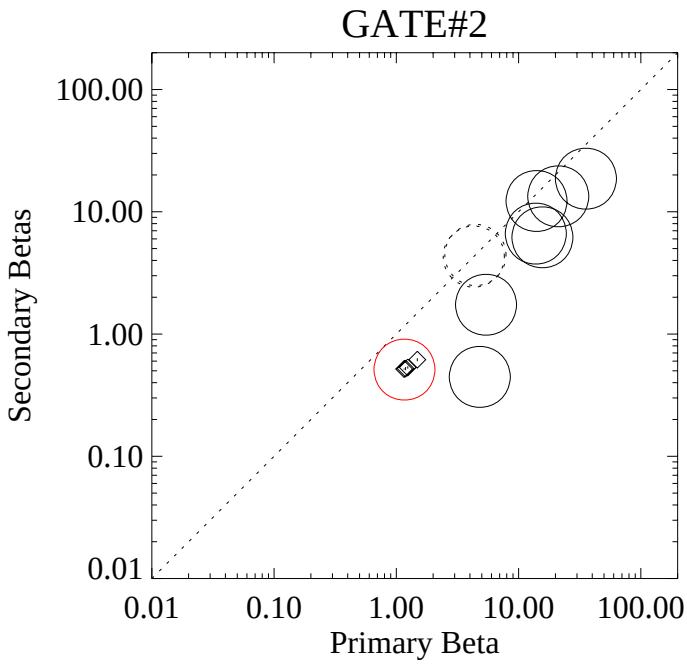
GATE#2
Secondary Betas
Primary Beta
100.00
10.00
1.00
0.10
0.01
0.01
0.10
1.00
10.00
100.00

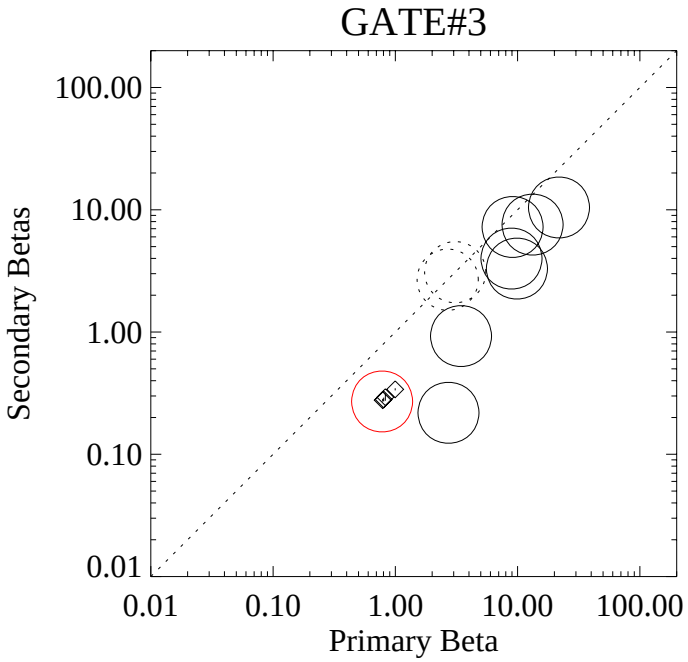
GATE#3
Secondary Betas
Primary Beta
100.00
10.00
1.00
0.10
0.01
0.01
0.10
1.00
10.00
100.00

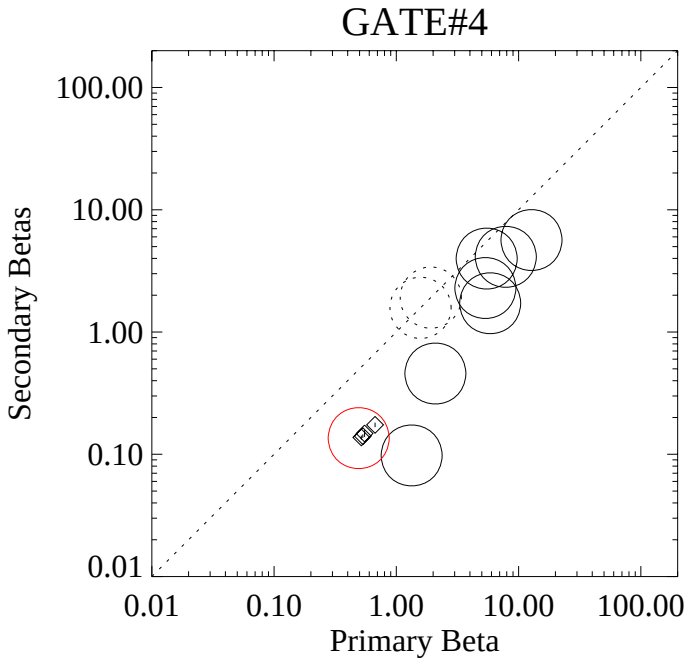
GATE#4
Secondary Betas
Primary Beta
100.00
10.00
1.00
0.10
0.01
0.01
0.10
1.00
10.00
100.00

APPENDIX C – DATA DIAGNOSTIC PLOTS FOR EM61 HH & TEMPLATE POSITIONING

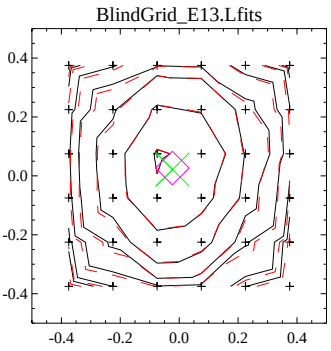
BlindGrid_E13.Lfits
0.4
0.2
0.0
-0.2
-0.4
-0.4
-0.2
0.0
0.2
0.4

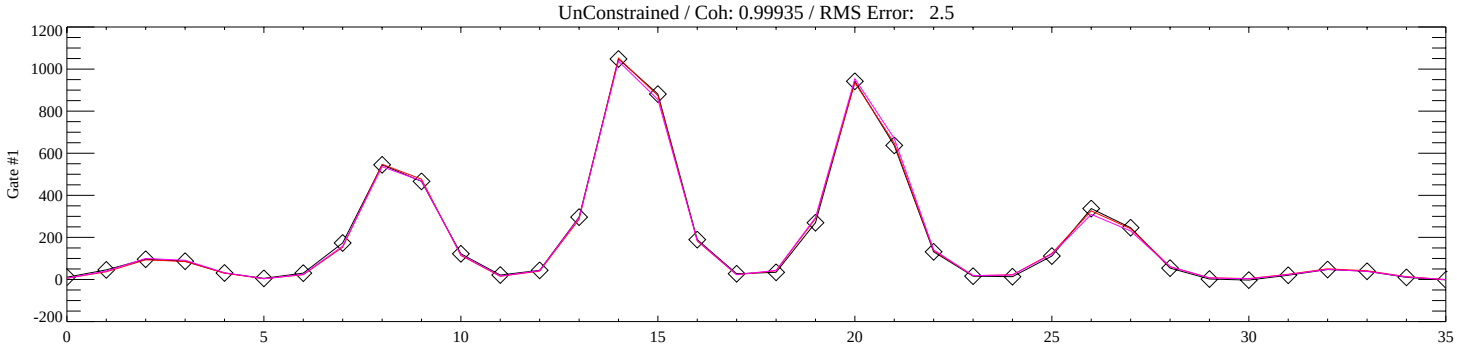
UnConstrained / Coh: 0.99935 / RMS Error: 2.5
Gate #1
1200
1000
800
600
400
200
0
-200
0
5
10
15
20
25
30
35

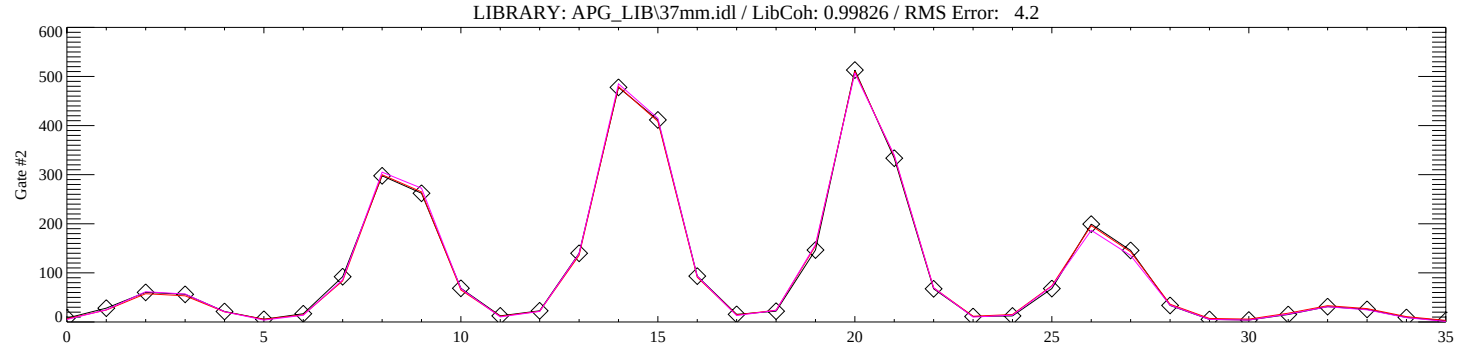
LIBRARY: APG_LIB\37mm.idl / LibCoh: 0.99826 / RMS Error: 4.2
Gate #2
600
500
400
300
200
100
0
0
5
10
15
20
25
30
35

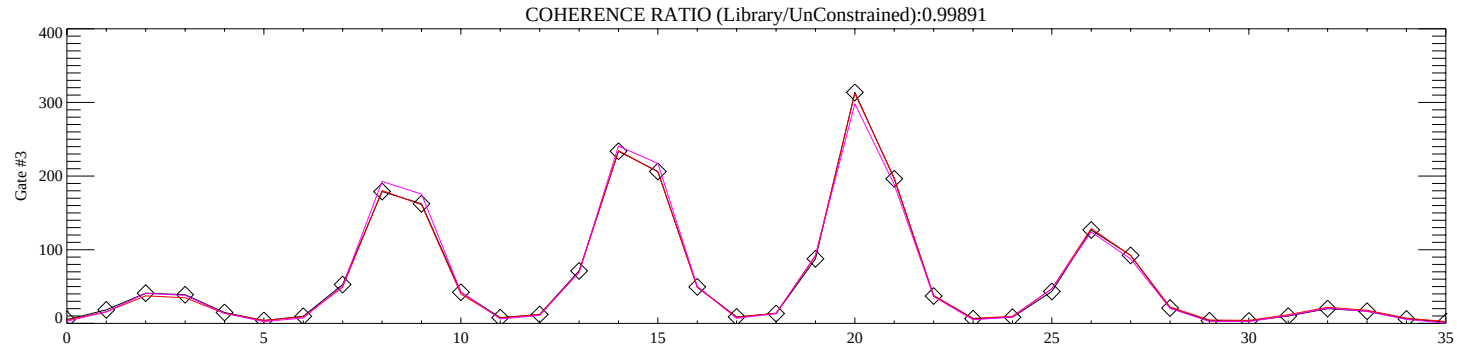
COHERENCE RATIO (Library/UnConstrained):0.99891
Gate #3
400
300
200
100
0
0
5
10
15
20
25
30
35

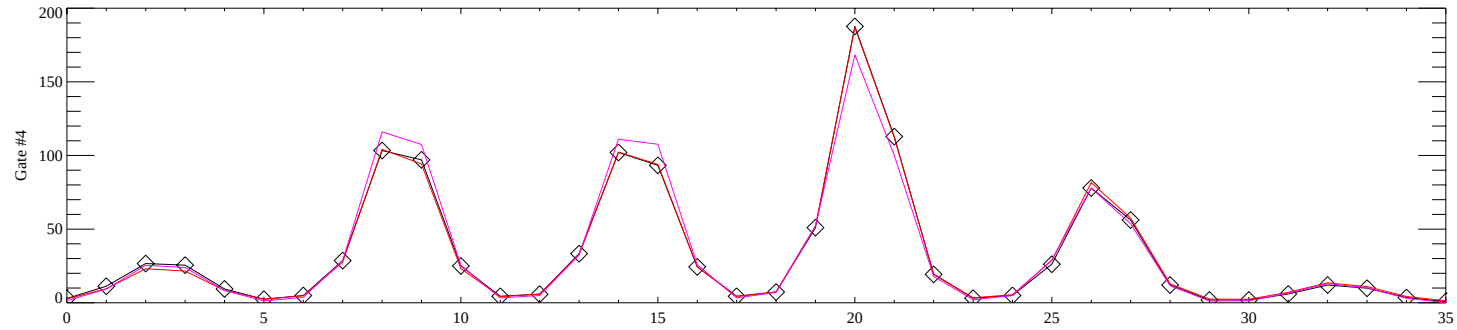
Gate #4
200
150
100
50
0
0
5
10
15
20
25
30
35

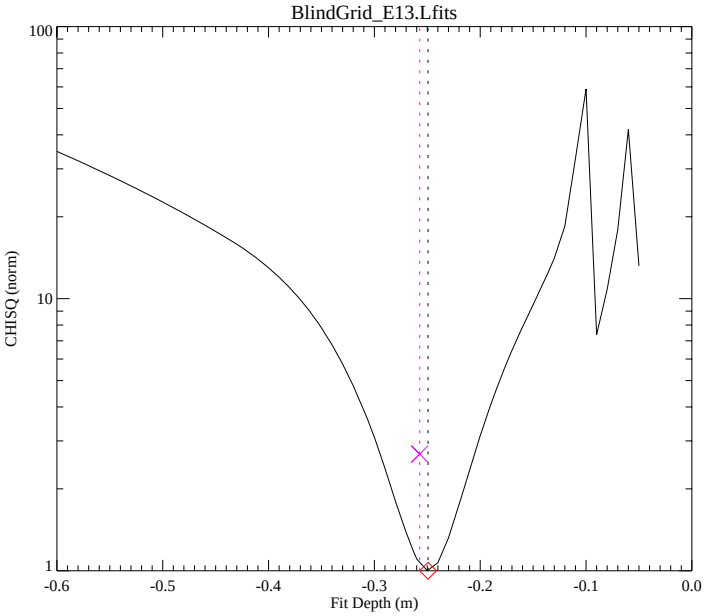
BlindGrid_E13.Lfits
CHISQ (norm)
Fit Depth (m)

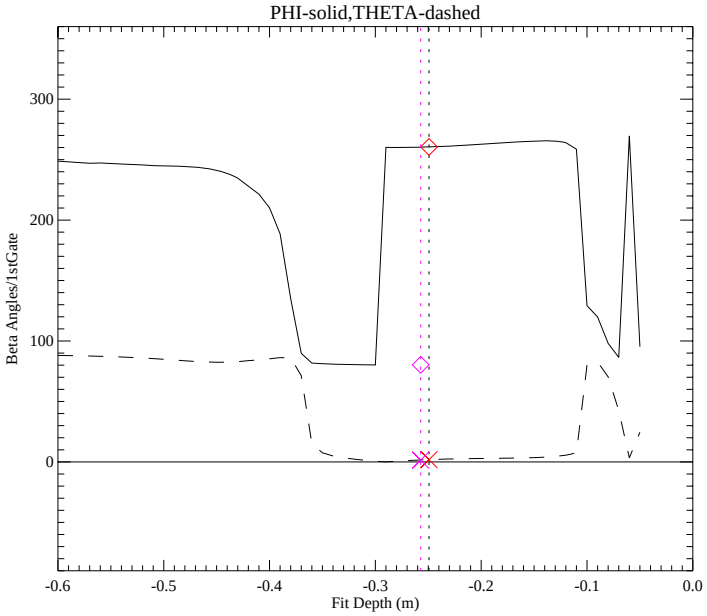
PHI-solid,THETA-dashed
Beta Angles/1stGate
Fit Depth (m)

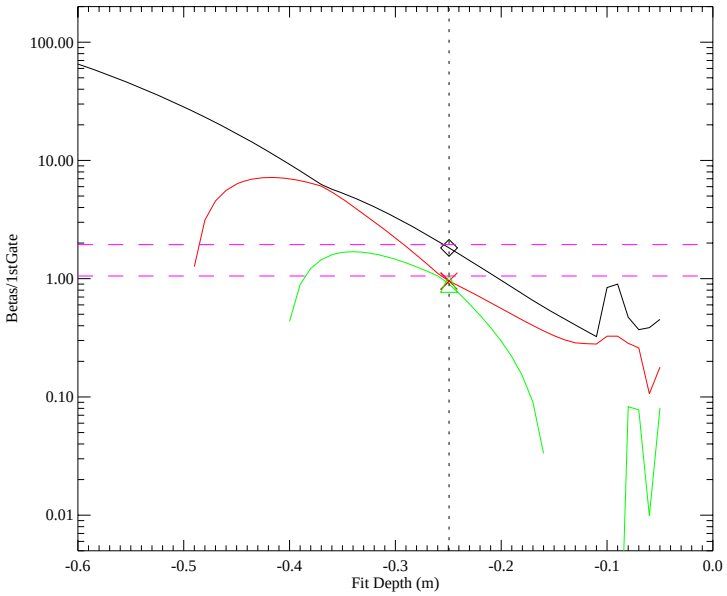
Betas/1stGate
Fit Depth (m)

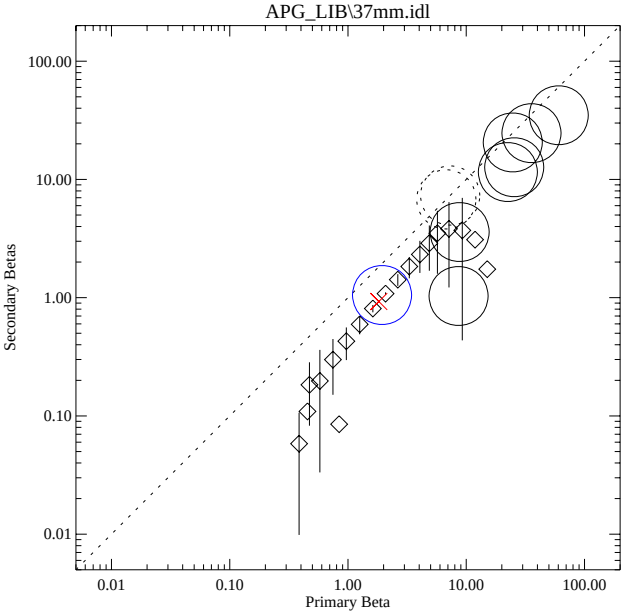
APG_LIB\37mm.idl
Secondary Betas
Primary Beta

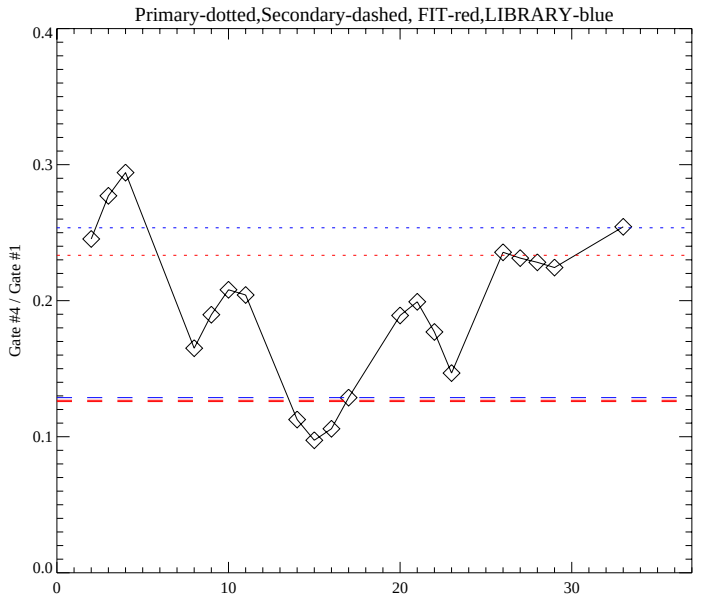
Primary-dotted,Secondary-dashed, FIT-red,LIBRARY-blue
Gate #4 / Gate #1

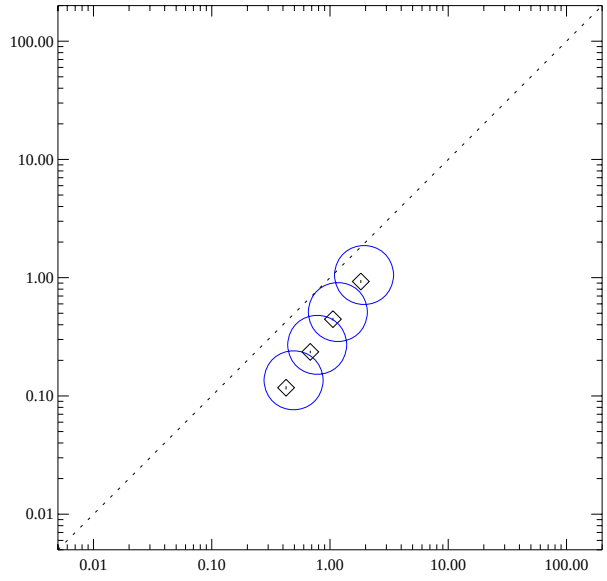

APPENDIX D – APG SCORING RESULTS

SAIC (July 2009)

TABLE 6a. BLIND GRID TEST AREA RESULTS (Template – Normal Scoring)

Response Stage					Discrimination Stage			
Munitions[a] Scores	P_d^{res}: by type				P_d^{disc}: by type			
	All Types	**105-mm**	**81/60-mm**	**37/25-mm**	**All Types**	**105-mm**	**81/60-mm**	**37/25-mm**
	0.99 0.97 0.93	0.98 0.93 0.83	1.00 0.97 0.88	1.00 1.00 0.93	0.93 0.89 0.83	0.94 0.87 0.75	0.94 0.87 0.75	0.98 0.93 0.83
By Depth[b]								
0 to 4D	1.00	1.00	1.00	1.00	0.90	0.95	0.88	0.86
4D to 8D	1.00	1.00	1.00	1.00	0.97	1.00	1.00	0.95
8D to 12D	0.67	0.67	0.00	1.00	0.56	0.50	0.00	1.00
Clutter Scores	P_{cd}				P_{fp}			
By Mass								
By Depth[b]	**All Mass**	**0 to 0.25 kg**	**>0.25 to 1 kg**	**>1 to 8 kg**	**All Mass**	**0 to 0.25 kg**	**>0.25 to 1 kg**	**>1 to 8 kg**
All Depth	1.00 1.00 0.98	1.00	1.00	1.00	0.35 0.29 0.24	0.12	0.42	0.60
0 to 0.15 m	1.00	1.00	1.00	1.00	0.30	0.13	0.47	0.50
0.15 to 0.3 m	1.00	1.00	1.00	1.00	0.25	0.00	0.14	0.75
0.3 to 0.6 m	N/A	N/A	N/A	N/A	N/A	N/A	N/A	N/A
Background Alarm Rates								
P_{ba}^{res}: 0.42					P_{ba}^{disc}: 0.14			

[a]The two numbers to the right of the all types munitions result are an upper and lower 90-percent confidence interval for an assumed binomial distribution.

[b]All depths are measured to the center of the object.

TABLE 7a. BLIND GRID EFFICIENCY AND REJECTION RATES (Template – Normal Scoring)

	Efficiency (E)	False Positive Rejection Rate	Background Alarm Rejection Rate
At Operating Point	0.92	0.71	0.66
With No Loss of P_d	1.00	0.31	0.60

TABLE 8a. BLIND GRID CORRECT TYPE CLASSIFICATION OF TARGETS CORRECTLY DISCRIMINATED AS MUNITIONS (Template – Normal Scoring)

Size	Percentage Correct
25/37mm	93%
60/81mm	87%
105mm	73%
Overall	84%

TABLE 9a. BLIND GRID MEAN LOCATION ERROR AND STANDARD DEVIATION (Template – Normal Scoring)

	Mean	Standard Deviation
Northing	--	--
Easting	--	--
Depth	0.095	0.039

TABLE 6a. BLIND GRID TEST AREA RESULTS (Saint – Normal Scoring)

Response Stage					Discrimination Stage			
Munitions[a] Scores	P_d^{res}: by type				P_d^{disc}: by type			
	All Types	**105-mm**	**81/60-mm**	**37/25-mm**	**All Types**	**105-mm**	**81/60-mm**	**37/25-mm**
	0.99 0.97 0.93	0.98 0.93 0.83	1.00 0.97 0.88	1.00 1.00 0.93	0.99 0.97 0.93	0.98 0.93 0.83	1.00 0.97 0.88	1.00 1.00 0.93
By Depth[b]								
0 to 4D	1.00	1.00	1.00	1.00	1.00	1.00	1.00	1.00
4D to 8D	1.00	1.00	1.00	1.00	1.00	1.00	1.00	1.00
8D to 12D	0.67	0.67	0.00	1.00	0.67	0.67	0.00	1.00
Clutter Scores	P_{cd}				P_{fp}			
By Mass								
By Depth[b]	**All Mass**	**0 to 0.25 kg**	**>0.25 to 1 kg**	**>1 to 8 kg**	**All Mass**	**0 to 0.25 kg**	**>0.25 to 1 kg**	**>1 to 8 kg**
All Depth	1.00 1.00 0.98	1.00	1.00	1.00	0.43 0.37 0.31	0.16	0.52	0.80
0 to 0.15 m	1.00	1.00	1.00	1.00	0.35	0.13	0.53	0.83
0.15 to 0.3 m	1.00	1.00	1.00	1.00	0.50	0.40	0.43	0.75
0.3 to 0.6 m	N/A	N/A	N/A	N/A	N/A	N/A	N/A	N/A
Background Alarm Rates								
	P_{ba}^{res}: 0.42				P_{ba}^{disc}: 0.16			

[a]The two numbers to the right of the all types munitions result are an upper and lower 90-percent confidence interval for an assumed binomial distribution.
[b]All depths are measured to the center of the object.

TABLE 7a. BLIND GRID EFFICIENCY AND REJECTION RATES (Saint – Normal Scoring)

	Efficiency (E)	False Positive Rejection Rate	Background Alarm Rejection Rate
At Operating Point	1.00	0.63	0.63
With No Loss of P_d	1.00	0.63	0.63

TABLE 8a. BLIND GRID CORRECT TYPE CLASSIFICATION OF TARGETS CORRECTLY DISCRIMINATED AS MUNITIONS (Saint – Normal Scoring)

Size	Percentage Correct
25/37mm	100%
60/81mm	97%
105mm	77%
Overall	91%

TABLE 9a. BLIND GRID MEAN LOCATION ERROR AND STANDARD DEVIATION (Saint – Normal Scoring)

	Mean	Standard Deviation
Northing	--	--
Easting	--	--
Depth	0.122	0.060

Appendix E: Points of Contact

POINT OF CONTACT	ORGANIZATION	Phone Fax e-mail	Role in Project
Dr. Herb Nelson	ESTCP Program Office Arlington, VA 22203	702-767-3686 (V) 202-215-4844 (C) herbert.nelson@osd.mil	Program Manager, MM
Ms. Katherine Kaye	HydroGeoLogic, Inc. Reston, VA 20190	410-884-4447 (V) kkaye@hgl.com	Program Manager Assistant, MM
Dr. Dean Keiswetter	SAIC Cary, NC 27513	919-677-1560 (V) 919-454-3212 (C) dean.a.keiswetter@saic.com	Principal Investigator
Mr. Glenn Harbaugh	Army Research Lab Welcome, MD 20693	804-761-5904 (V) roo749@yahoo.com	Site Safety Officer
Dr. Bruce Barrow	SAIC Arlington, VA 22202	703-414-3884 (V) bruce.j.barrow@saic.com	Data Analysis
Mr. Rick Fling	Aberdeen Test Center	410-278-2999 (V) 301-992-9080 (C) rick.fling@us.army.mil	Test Site Manager